One-dimensional transport in hybrid metal-semiconductor nanotube systems

M. F. Gelin and I. V. Bondarev

Phys. Rev. B **93**, 115422 — Published 16 March 2016

DOI: 10.1103/PhysRevB.93.115422

One-dimensional transport in hybrid metal-semiconductor nanotube systems

M. F. Gelin
Department of Chemistry, Technische Universität München, D-85747 Garching, Germany

I. V. Bondarev*
Department of Mathematics and Physics, North Carolina Central University, Durham, NC 27707, USA

We develop an electron transport theory for the hybrid system of a semiconducting carbon nanotube that encapsulates a one-atom-thick metallic wire. The theory predicts Fano resonances in electron transport through the system, whereby the interaction of electrons on the wire with nanotube plasmon generated near-fields blocks some of the wire transmission channels to open up the new coherent plasmon-mediated channel in the nanotube forbidden gap outside the wire transmission band. Such a channel makes the entire hybrid system transparent in the energy domain where neither wire, nor nanotube is indivudually transparent. This effect can be used to control and optimize charge transfer in hybrid nanodevices built on metal-semiconductor nanotube systems.

I. INTRODUCTION

Over the last decade, electron transport studies in quasi-one-dimensional (1D) nanostructures have resulted in important discoveries, such as conductance quantization and oscillatory length dependence, molecular rectification, negative differential resistance, hysteresis behavior, etc.[1–4] At present, peculiar mechanisms of electron transport are fairly well understood for pristine atomic wires (AWs)[1], carbon nanotubes (CNs) and some CN based components[4,5]. Carbon nanotubes — graphene sheets rolled-up into cylinders of one to a few nanometers in diameter and up to hundreds of microns in length[6] — have been successfully integrated into miniaturized electronic, electromechanical, chemical devices and into nanocomposite materials[7,8], and have found a variety of applications in optoelectronics[9–17].

Enormous potential of carbon nanotubes as building blocks for designing optoelectronic nanodevices stems from their extraordinary thermomechanical stability combined with unique physical properties that originate from quasi-one-dimensionality to give rise to a peculiar quasi-1D band structure featuring intrinsic, spatially confined, collective electronic excitations such as excitons and plasmons[18–23]. Due to the circumferential quantization of the longitudinal electron motion, the real parts of the axial (along the CN axis) optical conductivities of single wall CNs consist of series of peaks $E_{11}, E_{22}, ...$, representing the first, second, etc. excitons, respectively [see Fig. 1 (a)]. The imaginary parts of the conductivities are linked with the real ones by the Kramers-Kronig relation, and so the real parts of the *inverse* conductivities show the resonances $P_{11}, P_{22}, ...$ next to their excitonic counterparts. These are weakly dispersive, low-energy ($\sim 1-2$ eV) inter-band plasmon modes. They were observed experimentally quite a while ago[20], and were theoretically demonstrated quite recently to play the key role in a variety of new surface electromagnetic (EM) phenomena with CNs[22–36], such as exciton-plasmon coupling[22,23], plasmon generation by excitons[24,25], exciton Bose-Einstein condensation in individual single wall CNs[26], Casimir attraction in double wall CNs[23,27,28], van der Waals coupling[29,30], spontaneous emission[30,31], resonance absorption[32], scattering[33], bipartite entanglement in hybrid systems of extrinsic atoms/ions doped into CNs[34–36], to mention a few, — all of relevance to conceptually new tunable optoelectronic device applications with CNs[37–39].

Apparently, further progress in CN optoelectronics can be expected from the exploration of complex hybrid CN structures[40,41], particularly, CNs doped with extrinsic species such as molecules[42–45], semiconductor quantum dots[10,46,47], atoms and ions[45,48–50], and also AW-encapsulating CNs[51–67]. This research direction is being pursued by a number of groups worldwide. Carbon nanotubes of different diameters are synthesized to host various metallic AWs, including Cr[55], Fe[56], Co[57], Ni[58], Cu[59], Ge[60], I[61], La[62], Gd[63], Mo[64,65], Eu[66], and Cs[67]. Quantum chemistry simulations are performed for the electronic structure of AW-encapsulating CNs[68–76], supplemented with electron transmission calculations for CNs encapsulating Gd/Eu[74], Mo[75] and Au-V(Cr)[76] AWs. However, the inter-play between the intrinsic 1D conductance of an atomic wire and CN plasmon mediated near-fields is still far from being well understood, calling for deeper theoretical insight into electron transport peculiarities in these complex hybrid quasi-1D quantum systems.

Encapsulating metallic wires of just one atom thick into a single wall CN, metallic or semiconducting, is known to drastically alter the transport properties of the compound hybrid system. The whole body of available data shows that transport peculiarities in hybrid CN–AW systems cannot be explained by a mere addition of the properties of pristine CNs and AWs, suggesting a crucial role of the CN–AW interactions with a variety of associated quantum interference effects, including opening extra (collective) transport channels[66,74–76]. For example, metallic single wall CNs encapsulating Eu atomic wires are experimentally demonstrated to have extra conduction channels to supplement an overall "Tomonaga-Luttinger liquid"-like transport behavior[66], and with both CNs and AWs being non-metals their compound

CN–AW hybrids are theoretically predicted to be metallic for CNs of appropriately chosen diameters[75].

Pristine metallic single wall CNs are excellent conductors by themselves[5], and so, theoretically, there is no surprise about extra channels in the CN transport that emerge upon encapsulating metal AWs into them. From theoretical perspective, more interesting is a hybrid system of metal-atomic-wire encapsulating *semiconducting* CNs. In these systems, at low bias voltages not exceeding the CN fundamental band-gap, the CN itself does not have any intrinsic open channels to conduct electrons. Hence, there is no electron exchange between the CN and the metallic AW encapsulated into it, with the transport being totally dominated by the AW alone, while at the same time being affected by local quasi-static fields of nanotube's collective interband plasmon excitations.

As an example, Fig. 1 shows same scale energy dependences for characteristic parameters to represent semiconducting CNs, their near-field interaction with encapsulated atomic types species, and one-dimensional (1D) metallic atomic wires, respectively. Panel (a) shows the dynamical axial conductivities for the semiconducting (11,0) and (16,0) CNs. Shown are the real and imaginary parts of the conductivities as well as the real parts of the inverse conductivities of relevance to the electron energy-loss spectroscopy response function used in studies of collective plasmon excitations in solids[20–23,77]. Peaks of the real parts of the conductivities and of the inverse conductivities represent excitons (E_{11}, E_{22}) and interband plasmons (P_{11}), respectively[22–28]. Panel (b) shows local densities of photonic states (DOS) for the non-radiative spontaneous decay (relative to vacuum) of a two-level dipole emitter placed on the symmetry axis (inset) inside the (11,0) and (16,0) CNs. Panel (c) shows the electron transmission band for the free 1D metallic AW of 100 sodium atoms with energy counted from the bottom of the fundamental band gap of the (11,0) and (16,0) CNs (top and bottom, respectively). All AW transport channels are seen to be inside of the CN forbidden gap. However, AWs encapsulated into CNs will experience near-field EM coupling to the CN interband plasmon modes represented by the large DOS resonances in panel (b). Interband plasmons are *standing* charge density waves due to the periodic opposite-phase displacements of the electron shells with respect to the ion cores in the neighboring elementary cells on the CN surface. Such periodic displacements induce local coherent oscillating electric fields of zero mean, but nonzero mean-square magnitude, concentrated near the surface across the diameter throughout the length of the CN[24,25]. The electric dipole interaction of atoms on the wire with these near-fields will largely affect the AW transmission properties and the properties of the entire hybrid system.

The coupling strength of an individual atom to the plasmon-induced near-fields inside the nanotube can be estimated as follows. Modeled by a two-level system, an atom (ion) interacts with the CN medium-assisted fields via an electric dipole transition $d_z = \langle u|\hat{d}_z|l\rangle$ between its

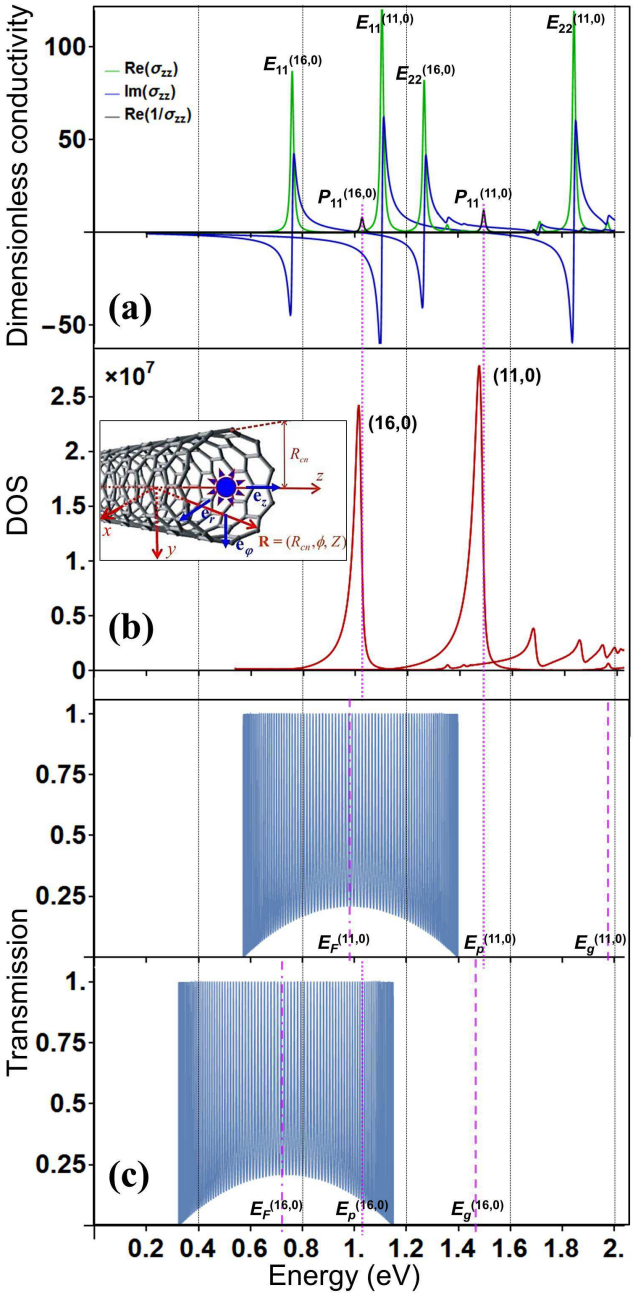

FIG. 1: (Color online) (a) Dimensionless (normalized by $e^2/2\pi\hbar$) surface axial conductivities σ_{zz} for the semiconducting (11,0) and (16,0) CNs. Peaks of $\mathrm{Re}\,\sigma_{zz}$ and $\mathrm{Re}(1/\sigma_{zz})$ represent excitons (E_{11}, E_{22}) and interband plasmons (P_{11}), respectively. (b) Photonic DOS for non-radiative spontaneous decay with CN plasmon excitation for a two-level dipole emitter on the symmetry axis (inset) of the (11,0) and (16,0) CN. (c) Electron transmission band for the *free* AW of 100 sodium atoms with energy counted from the bottom of the fundamental band gap E_g of the (11,0) and (16,0) CNs (top and bottom, respectively); also shown are the AW Fermi energies E_F and CN first interband plasmon energies E_p. Conductivities are obtained using the $(\mathbf{k}\cdot\mathbf{p})$-scheme by Ando[18]. DOS functions are calculated as described by Bondarev and Lambin in Refs.[29,30]. Transmission is plotted within the nearest-neighbor hopping model as discussed by Mujica *et al.* and by Gelin and Kosov in Refs.[87–89]. See Sec. V for more details.

lower $|l\rangle$ and upper $|u\rangle$ states[29,30], with the CN symmetry axis set to be the z-quantization axis [Fig. 1(b), inset]. Transverse dipole orientations can be neglected in view of the strong transverse depolarization in individual CNs[21,78–80]. The atom–CN electric dipole coupling constant is then given by $\hbar g = (2\pi d_z^2 \hbar\tilde{\omega}_A/\tilde{V})^{1/2}$[32,82], where $\tilde{\omega}_A$ is the effective transition frequency *in resonance* with a local CN-medium-assisted field mode. The effective mode volume $\tilde{V} \sim \pi R_{CN}^2(\tilde{\lambda}_A/2)$ for the CN of radius R_{CN}. Evaluating $d_z \sim e r_A \sim e(e^2/\hbar\tilde{\omega}_A)$, where r_A is the linear size of the atom (estimate valid for quantum systems with Coulomb interaction[81]), and introducing the fine structure constant $\alpha = e^2/\hbar c = 1/137$, one arrives at $\hbar g = (2\alpha^3/\pi)^{1/2}(\hbar c/R_{CN})$, to give $\hbar g \sim 0.2$ eV for CNs with diameters ~ 1 nm. Comparing this to the "cavity" linewidth $\hbar\gamma_c(\tilde{\omega}_A) = 6\pi\hbar c^3/\tilde{\omega}_A^2 \xi(\tilde{\omega}_A)\tilde{V}$ [function ξ represents the local photonic DOS at the atomic location, also called the Purcell factor[82]; shown in Fig. 1(b)], one has the ratio $g/\gamma_c \sim 10 \gg 1$ for the 1 nm-diameter CNs in the optical spectral range. This is the strong atom-field coupling condition characterized by the rearrangement ("dressing") of atomic levels and formation of atomic quasi-1D cavity polaritons[29,30] featuring strongly non-exponential (oscillatory) spontaneous decay dynamics[30,31] and Rabi splitting of the optical absorption line profile[32]. However, one can hardly expect such a strong resonance coupling for identical atoms aligned on a wire inside the CN as the $|l\rangle$ and $|u\rangle$ transition states are here a subset of the one-dimensional electronic band states, and so are not as clearly defined as those for an individual atom, to most likely result in a weaker *non-resonance* CN–AW coupling strength.

Here we study the inter-play between the intrinsic 1D conductance of metallic AWs and CN mediated near-field effects for *semiconducting* single wall CNs that encapsulate atomic wires of finite length. We use the matrix Green's functions formalism to develop an electron transfer theory for such a complex hybrid quasi-1D CN system. The theory predicts Fano resonances in electron transmission through the system. That is the AW–CN near-field interaction blocks some of the pristine AW transmission band channels to open up new coherent channels in the CN forbidden gap outside the pristine AW transmission band. This makes the entire hybrid system transparent in the energy domain where neither of the individual pristine constituents, neither AW nor CN, is transparent. The effect can be used to control electron charge transfer in semiconducting CN based devices for nanoscale energy conversion, separation and storage[83–86].

The paper is structured as follows. Section II formulates the theoretical model for CN-mediated AW transmission. Section III presents analytical expressions derived for the transmission coefficient. The expressions obtained are analyzed qualitatively in Section IV, and then numerically in Section V. Section VI discusses the model approach and the approximations used. A brief summary of the work is given in Section VII. Appendix A derives mathematical expressions presented in Section III.

II. THE MODEL

This Section formulates the model for the plasmon-mediated electron transport through the hybrid metal AW encapsulating single wall semiconductor CN system. We closely follow the matrix Green's function formalism by Mujica, Kemp and Ratner[87,88] (see also Ref.[89]), which is consistently built on the scattering matrix approach (see, e.g., Refs.[4,81]) as applied to electron conduction in molecular wires. This formalism is exact in the limit of low temperature and small external bias applied, whereby the system under consideration is in the linear response regime characterized by the bias independent T-matrix of the transported electrons. The latter is defined as $T(\mathcal{E}) = S(\mathcal{E}) - 1 = V + VG(\mathcal{E})V$ with $\mathcal{E}$ standing for the complex energy, S and V being the electron scattering matrix and scattering potential, respectively, and $G(\mathcal{E}) = 1/(\mathcal{E} - \mathcal{H})$ representing the Green's function with $\mathcal{H}$ being the Hamiltonian of the entire system to include both the electron reservoirs (leads, electrodes) and the wire connecting them.

The quantum conductance of the wire–reservoir system is defined as the ratio of the current density to the applied voltage, $\mathrm{g} = j/W$. This only depends on the electronic structure of the wire and reservoirs in this model, while being completely independent of the voltage. For the wire modeled by a chain of N one-electron states, the conductance g can be shown to be represented by the wire-reservoir transmission coefficient (in units of $e^2/2\pi\hbar$)

$$T(E) = 4\Delta_1(E)\Delta_N(E)\,|G_{1N}(E)|^2 \tag{1}$$

taken at $E = \epsilon_F$, where E is the real part of the complex energy $\mathcal{E}$ and ϵ_F is the Fermi energy of the reservoirs (leads, electrodes)[87,88]. The transmission coefficient is the probability for an electron to be transported between the electrodes at a constant energy E, whereby $0 \le T(E) \le 1$. The function $G_{1N}(E)$ is the $1N$ element of the wire–reservoir Green's function matrix

$$\mathbf{G}(E) = [E - \mathbf{H} - \mathbf{\Sigma}(E)]^{-1}, \tag{2}$$

in which $\mathbf{H}$ stands for the Hamiltonian matrix of the wire *alone*, and

$$\mathbf{\Sigma}(E) = \mathbf{\Lambda}(E) - i\mathbf{\Delta}(E) \tag{3}$$

stands for the electron reservoir self-energy matrix to take into account the lead–wire coupling. This only has two non-zero matrix elements to couple the left and right wire terminals to the left and right reservoirs. They are $\Sigma_{11}(E) = \Lambda_1 - i\Delta_1$ and $\Sigma_{NN}(E) = \Lambda_N - i\Delta_N$, where $\Delta_{1,N}(E)$ and $\Lambda_{1,N}(E)$ are the reservoir spectral densities of states and their Hilbert transforms, respectively.

In the case where the left and right reservoirs (leads, electrodes) are identical, one has $\Sigma_{11} = \Sigma_{NN} = \Lambda - i\Delta$. Then, the transmission coefficient (1) takes the form

$$T(E) = 4\Delta^2(E)\,|G_{1N}(E)|^2. \tag{4}$$

If, moreover, the identical leads are made of a broadband metal with the half-filled conduction band, then it can be shown (see Ref.[88] for details) that $\Lambda(E)=0$ for the most interesting E in the neighborhood of ϵ_F, while $\Delta(E)$ takes the energy independent form $\Delta = V_S^2/\gamma$, where V_S $(=V_1 \equiv V_N)$ is the lead–wire terminal chemisorption coupling constant and γ is the lead metal half-bandwidth.

The ultimate goal of this work is to derive the equation for and analyze the energy dependence of the transmission coefficient $T(E)$ for the hybrid metal-semiconductor nanotube system composed of the metal AW encapsulated in the semiconducting CN.

A. The Hamiltonian of the hybrid CN–AW system

According to Eqs. (1)–(4), the main ingredient of the electron transmission theory of molecular wires in its scattering matrix formulation is the Green's function of the wire-reservoir system in Eq. (2). This includes the separate contributions from the Hamiltonian of the wire *alone* and from the electron reservoir self-energy to account for the wire–lead coupling. Our "wire" is the hybrid metal-semiconductor nanotube system composed of the metal AW encapsulated in the semiconducting CN. We write the total Hamiltonian for our system as the sum of the Hamiltonians for the AW, the CN, and their interaction as follows

$$\hat{H} = \hat{H}_{\rm AW} + \hat{H}_{\rm CN} + \hat{H}_{\rm int}. \tag{5}$$

To describe the AW of N atoms (lattice sites) in length, we adopt the standard second quantized tight-binding model Hamiltonian with the nearest neighbor electron hopping rate V and the electron on-site energy E_0,

$$\hat{H}_{\rm AW} = E_0 \sum_{k=1}^{N} B_k^\dagger B_k + V \sum_{k=1}^{N-1} \left(B_k^\dagger B_{k+1} + B_{k+1}^\dagger B_k \right). \tag{6}$$

Here, the operators $B_k^\dagger$ and B_k create and annihilate, respectively, the single-quantum electronic excitations on site k of the AW. They obey the Pauli commutation rules $[B_k, B_n^\dagger] = \delta_{kn}(1 - 2B_k^\dagger B_n)$, whereby no two electrons can occupy the same lattice site simultaneously, though being able to occupy equivalent neighboring lattice sites at the same time. This Hamiltonian is the simplest one to capture the essence of the near-field EM effects we are about to study and discuss, the effects to occur inside the fundamental bandgap $E_g\,[=E_g^{(11)}]$ of the semiconducting CN at the energies $E_F \lesssim E < E_g$, where E_F is the Fermi energy of the AW as it shows in Fig. 1 (a)–(c). Here, regardless of whether the AW transmission band is narrower [as in Fig. 1 (c)] or broader than E_g, the near-field electric dipole interaction that involves electronic dipole transitions in the atoms on the wire due to the energy exchange with the quasi-static near-fields of low-energy ($\sim 1-2$ eV) collective interband plasmon modes of the nanotube [represented by the local photonic DOS resonances in Fig. 1 (b)], will largely affect the AW electron transmission and thereby the transport properties of the entire hybrid metal-semiconductor nanotube system.

The most general second quantized Hamiltonian of the CN can be written as follows (Ref.[22])

$$\hat{H}_{\rm CN} = \sum_{\mathbf{n}} \int_0^\infty d\omega\, \hbar\omega \hat{f}^\dagger(\mathbf{n},\omega)\hat{f}(\mathbf{n},\omega). \tag{7}$$

In this Hamiltonian, the scalar bosonic field operators $\hat{f}^\dagger(\mathbf{n},\omega)$ and $\hat{f}(\mathbf{n},\omega)$ create and annihilate, respectively, the surface EM excitation (plasmon) of frequency ω at an arbitrary point $\mathbf{n} = \mathbf{R}_n = \{R_{CN}, \varphi_n, z_n\}$ that represents the position of a carbon atom [nanotube lattice site — Fig. 1 (b), inset] on the surface of the CN of radius R_{CN}, $[\hat{f}(\mathbf{n},\omega), \hat{f}^\dagger(\mathbf{n}',\omega')] = \delta_{\mathbf{nn}'}\delta(\omega-\omega')$. Summation is taken over all the carbon atoms on the entire CN surface. Since only one plasmon resonance is located inside E_g, Eq. (7) can further be simplified to take the form

$$\hat{H}_{\rm CN} = E_p\, \hat{f}^\dagger \hat{f}. \tag{8}$$

Here, the operators $\hat{f}^\dagger$ and $\hat{f}$ ($[\hat{f}, \hat{f}^\dagger]=1$) create and annihilate *collective* interband plasmon excitations of energy E_p [Fig. 1 (a),(b)] that are delocalized all over the CN surface in accordance with the correspondence relation

$$\sum_{\mathbf{n}} \hat{f}^\dagger(\mathbf{n},\omega)\hat{f}(\mathbf{n},\omega) = \hat{f}^\dagger \hat{f}\, \delta(\omega - E_p/\hbar). \tag{9}$$

The CN–AW interaction can then be written in the form

$$\hat{H}_{\rm int} = \sum_{k=1}^{N} \mu_k \left(B_k \hat{f}^\dagger + B_k^\dagger \hat{f} \right), \tag{10}$$

where μ_k is the AW–CN dipole coupling constant for site k of the AW. We assume it to be the same for all of the AW sites, that is

$$\mu_k = \mu \lesssim \hbar g = \sqrt{\frac{2\pi d_z^2 \hbar\tilde{\omega}_A}{\tilde{V}}} \approx \sqrt{\frac{2\alpha^3}{\pi}}\frac{\hbar c}{R_{CN}} \tag{11}$$

in what follows, as discussed in the introduction above.

The Hamiltonian in Eqs. (5)–(11) belongs to the well-known family of Fano-Anderson Hamiltonians[90,91]. However, it describes a physical picture opposite to that normally refereed to as the Fano–Anderson model. The latter deals with a *bound* (e.g., localized on a defect) electron state inside (or outside) of the continuum of scattering (band, or free) electron states[90]. In our case, the band electron states represented by the AW Hamiltonian (6), interact with the CN collective interband plasmon excitations described by the Hamiltonian (8). These are standing charge density waves due to the periodic opposite-phase displacements of the electron shells with respect to the ion cores in the neighboring elementary cells on the CN surface[24,25]. They are *extended* coherently all over

the entire surface of the CN as described by Eqs. (7) and (9). The main feature of the standard Fano–Anderson model is still there though, offering two different electron transmission paths. They are: (i) the direct transfer through the AW, and (ii) the transfer mediated by quasi-static near-fields due to the CN collective interband plasmon excitations. Thus, the model we present here is a non-trivial extension of the Fano-Anderson model to cover coherently delocalized electron states, such as collective plasmon excitations, in addition to localized (defect-type) states studied originally.

B. The matrix representation of the operators

Using the relevant single-quantum Hilbert space basis of $N+1$ basis vectors as follows

$$\left\{B_k^\dagger\,|0\rangle\right\}_{k\,=1,\cdots,N}\,,\;\hat{f}^\dagger|0\rangle\,,$$

with $|0\rangle$ being the vacuum state of the entire system, one can convert the total Hamiltonian (5) into the matrix representation as follows

$$\mathbf{H}=\begin{bmatrix} E_0 & V & 0 & \dots & 0 & 0 & \mu \\ V & E_0 & V & \dots & 0 & 0 & \mu \\ 0 & V & E_0 & \dots & 0 & 0 & \mu \\ \vdots & \vdots & \vdots & \ddots & \vdots & \vdots & \vdots \\ 0 & 0 & 0 & \dots & E_0 & V & \mu \\ 0 & 0 & 0 & \dots & V & E_0 & \mu \\ \mu & \mu & \mu & \dots & \mu & \mu & E_p \end{bmatrix}. \tag{12}$$

Here, rows and columns $1,\dots,N$ enumerate AW sites. The $(N+1)$-st row/column refers to the CN interband plasmon mode. Similar matrix representations can be written for other operators of relevance to the problem.

Matrix (12) represents the tight-binding Hamiltonian for the hybrid CN–AW system. Its diagonal matrix elements $H_{11},\dots,H_{NN}$ are the site energies of the AW sites that incoming electrons hop through, its off-diagonal elements specify the rates at which the hopping occurs through the AW, and its eigen energies determine the resonances of the electron transmission through the CN–AW system. The AW–CN coupling constant μ in the $(N+1)$-st row/column modifies the resonance transmission energies and hopping pathways. To explore the role of this latter ingredient is the goal of this work.

III. THE TRANSMISSION COEFFICIENT: EXACT ANALYTICAL SOLUTION

For simplicity and to obtain tractable results, we derive the transmission coefficient $T(E)$ in the form (4) assuming identical leads made of a broadband metal with the half-filled conduction band as discussed above in Sec. II.

To evaluate the matrix element $G_{1N}(E)$ of the Green's function (2) in Eq. (4), we introduce the matrix

$$\mathbf{h}\equiv E-\mathbf{H}-\mathbf{\Sigma}(E),$$

and follow the rules for calculating the matrix elements of its inverse. One obtains

$$G_{1N}(E)=\frac{\mathbf{h}_{N1}}{\det(\mathbf{h})}, \tag{13}$$

with $\mathbf{h}_{N1}$ representing the $N1$ cofactor of the matrix $\mathbf{h}$. Next, we use the result of the matrix Green's function partitioning technique developed in Ref.[87], whereby

$$\det(\mathbf{h})=\Sigma^2 D_{N-2}+2\,\Sigma D_{N-1}+D_N \tag{14}$$

with $\Sigma=\Sigma_{11}=\Sigma_{NN}=-i\Delta\;(=-iV_S^2/\gamma)$, and

$$\mathbf{h}_{N1}=(-1)^{N+1}S_{N-1}, \tag{15}$$

with D_N and S_{N-1} being the determinant and the $N1$ minor of the matrix $\mathbf{H}-E$, respectively (both determined by the AW lattice site number N; subscripts to indicate that the latter is a polynomial of degree one less than the former). The matrix $\mathbf{H}$ is given by Eq. (12).

In view of Eqs. (13)–(15), the transmission coefficient (4) takes the form

$$T(E)=4\Delta^2\left|\frac{S_{N-1}}{\Delta^2 D_{N-2}+2i\Delta D_{N-1}-D_N}\right|^2. \tag{16}$$

Here, the quantities D_N and S_N are functions of the AW lattice site number N given by the analytical expressions as follows

$$D_N=\varepsilon_p\,d_N+ \tag{17}$$

$$\frac{\mu^2}{\varepsilon_0+2V}\left\{-Nd_N+\frac{2V}{\varepsilon_0+2V}\left[(-1)^N V^N-Vd_{N-1}-d_N\right]\right\},$$

$$S_N=\varepsilon_p V^N+\frac{\mu^2}{\varepsilon_0+2V}\left[-(N+1)V^N+(-1)^N d_N\right], \tag{18}$$

where

$$\varepsilon_0=E_0-E,\;\;\varepsilon_p=E_p-E\,, \tag{19}$$

and

$$d_N=\frac{\lambda_1^{N+1}-\lambda_2^{N+1}}{\lambda_1-\lambda_2} \tag{20}$$

with

$$\lambda_{1,2}=\frac{\varepsilon_0\pm\sqrt{\varepsilon_0^2-4V^2}}{2}\,. \tag{21}$$

The explicit derivation of Eqs. (17) and (18) can be found in Appendix A.

IV. QUALITATIVE ANALYSIS

The transmission coefficient given by Eqs. (16)–(21) is the key quantity to describe the electron transfer through the atomic wire encapsulated into a carbon nanotube. There are two parameters to control the AW–CN coupling there. They are the atom-plasmon coupling constant μ and the plasmon energy detuning ε_p in Eqs. (11) and (19), respectively. From Eqs. (17) and (18), we see that it is the ratio $\mu^2/\varepsilon_p = \mu^2/(E_p - E)$ that determines the $T(E)$ energy dependence. [The conductance g is determined by $\mu^2/(E_p - \epsilon_F)$, accordingly.] In view of this, increasing μ affects $T(E)$ the same way as decreasing ε_p, and vice versa. Therefore, we restrict ourselves to the analysis of the $T(E)$ behavior versus μ in what follows.

A. Pristine AWs

The pristine AW case follows from the general equation (16) if one substitutes $\mu = 0$ there. Then, we recover the known quantum wire transmission formula[87,89]

$$T(E) = 4\Delta^2 \left| \frac{V^{N-1}}{\Delta^2 d_{N-2} + 2i\Delta d_{N-1} - d_N} \right|^2 . \qquad (22)$$

This shows that there are two possible, qualitatively different electron transport regimes there for pristine AWs, depending on whether $|\varepsilon_0/2V| < 1$, or $|\varepsilon_0/2V| > 1$.

In the case where $|\varepsilon_0/2V| < 1$, the roots $\lambda_{1,2}$ of Eq. (21) are complex, yielding d_N in Eq. (20) of the form

$$d_N = \frac{\sin[(N+1)\phi]}{\sin\phi}\, V^N \qquad (23)$$

with ϕ given by the roots of the equation $\cos\phi = \varepsilon_0/2V$. In this case Eq. (22) takes the form

$$T(E) = \left| \frac{2\xi \sin\phi}{\sin[(N+1)\phi] + 2i\xi \sin(N\phi) - \xi^2 \sin[(N-1)\phi]} \right|^2$$

with $\xi = \Delta/V = (V_S/\gamma)(V_S/V) \ll 1$ since for broadband leads one would naturally expect the inequalities $V_S < \gamma$ and $V_S \lesssim V$ to be fulfilled. This is the resonance tunneling regime, in which the energies of the transmission maxima are *approximately* given by the roots of the equation $\sin[(N+1)\phi] = 0$ (corresponding to the minima of the denominator) as follows

$$\phi_k^{max} = \frac{\pi k}{N+1}, \quad k = 1, 2, \cdots, N, \qquad (24)$$

to result in the resonance transmission band of precisely N energy channels for the AW of N atoms in length. They are

$$E_k^{max} = E_0 - 2V\cos\phi_k^{max} = E_0 - 2V\cos\frac{\pi k}{N+1}\,,$$
$$T_k^{max} = T(E_k^{max}) = \frac{1}{1 + \xi^2 \cos^2\phi_k^{max}}\,. \qquad (25)$$

These transmission maxima channels interchange with transmission minima given approximately by the roots of the equations $\sin[(N+1)\phi] = \pm 1$ (corresponding to the maxima of the denominator)

$$\phi_k^{min} = \frac{\pi(k+1/2)}{N+1}, \quad k = 1, \cdots, N-1, \qquad (26)$$

yielding

$$E_k^{min} = E_0 - 2V\cos\phi_k^{min} = E_0 - 2V\cos\frac{\pi(k+1/2)}{N+1}\,,$$
$$T_k^{min} = T(E_k^{min}) = \frac{4\xi^2 \sin^2\phi_k^{min}}{\left[1 - \xi^2\cos 2\phi_k^{min}\right]^2 + 4\xi^2\cos^2\phi_k^{min}}. \qquad (27)$$

The magnitude of T_k^{min} is seen to increase with Δ (as long as $\xi = \Delta/V < 1$), thereby representing the strength of the coupling of the AW to the leads. For instance, $T_k^{min} = 4\xi^2/(1+\xi^2)^2$ for E_k^{min} in the center of the transmission band ($E_k^{min} = E_0$, whereby $\cos\phi_k^{min} = 0$), to give $T_k^{min} \approx (2\Delta/V)^2$ for $\Delta \ll V$ (weak AW-lead coupling) and $T_k^{min} \approx 1$ for $\Delta \sim V$ (strong AW-lead coupling).

In the case where $|\varepsilon_0/2V| > 1$, the roots $\lambda_{1,2}$ of Eq. (21) are real. Approximating them with their respective leading terms of the power series expansions in $|2V/\varepsilon_0| < 1$, one has $\lambda_{1,2} \approx (\varepsilon_0 \pm |\varepsilon_0|)/2$. Then, d_N in Eq. (20) is estimated to go asymptotically as

$$d_N \approx \varepsilon_0^N = (E_0 - E)^N.$$

The transmission coefficient (22) takes a non-resonant form then that scales with N exponentially,

$$T(E) \approx 4\xi^2 \Big(\frac{\varepsilon_0}{V}\Big)^{-2N} = 4\xi^2 \left(\frac{E_0 - E}{V}\right)^{-2N}, \qquad (28)$$

showing a fast exponential decrease as N increases. For $|\varepsilon_0/2V| \gtrsim 1$, on the other hand, $\lambda_{1,2} = (\varepsilon_0 \pm |\varepsilon_0|\epsilon)/2$ with $\epsilon = \sqrt{1 - (2V/\varepsilon_0)^2}$ now being a small positive parameter, to result in the leading term

$$d_N \approx (N+1)\left(\frac{\varepsilon_0}{2}\right)^N = (N+1)\left(\frac{E_0 - E}{2}\right)^N$$

of the power series expansion in ϵ. In this regime, the transmission coefficient (22) is an energy independent constant decreasing with N as follows

$$T(E) \approx \frac{4\xi^2}{(N+1)^2}\,.$$

This can also be obtained using Eq. (23) for $|\varepsilon_0/2V| \lesssim 1$.

B. Coupled CN–AW system

Non-zero μ changes drastically the electron transport through the coupled CN–AW system. Intuitively, one

would expect additional transmission resonances (Fano-like[91]) to appear in the transmission coefficient (4). In this section we analyze Eq. (16) qualitatively to show that this is indeed the case. This analysis is continued in Sections V and VI to discuss the numerical results.

Dividing the numerator and denominator of Eq. (16) by V^N, one obtains

$$T(E)=\left|\frac{2\xi\,\rho_{N-1}}{\xi^2\delta_{N-2}+2i\xi\,\delta_{N-1}-\delta_N}\right|^2, \qquad (29)$$

where $\rho_N = S_N/V^N$ and $\delta_N = D_N/V^N$. With $\xi \ll 1$, the transmission maxima are determined by the condition $\delta_N = 0$, to minimize the denominator. If $\mu = 0$, this becomes $d_N = 0$, according to Eq. (17), to bring us back to Eqs. (25) and (28) for $|\varepsilon_0/2V| < 1$ (resonance transmission band) and for $|\varepsilon_0/2V| > 1$ (exponentially small transmission domain), respectively. For $\mu \neq 0$ and $|\varepsilon_0/2V| > 1$, we see from Eq. (17) that there exists one more possibility to make δ_N close to zero. This is where $\varepsilon_p(\varepsilon_0 + 2V) = N\mu^2$, to result in two additional energy levels as follows

$$E_{1,2} = \frac{1}{2}\left[E_0 + 2V + E_p \pm \sqrt{(E_0 + 2V - E_p)^2 + 4N\mu^2}\right]. \qquad (30)$$

As the top and bottom edges of the pristine AW tunneling band are given by $E = E_0 \pm 2V$ [see Eq. (25)], the E_1 (higher energy) level falls into the domain $E > E_0+2V$ (or $\varepsilon_0/2V < -1$) of the exponentially small transmission of the pristine AW, thereby *opening* an extra transmission channel in this opaque area. At fixed $\mu \neq 0$, raising in energy with N, this channel stays within the CN forbidden gap as long as $N\mu^2 < (E_g - E_p)(E_g - E_0 - 2V)$, crossing into the CN conduction band when the inequality changes its sign. The E_2 (lower energy) level falls into the resonance tunneling band $E_0 - 2V < E < E_0 + 2V$ (or, equivalently, $|\varepsilon_0/2V| < 1$) of the pristine AW and remains there as long as the inequality $N\mu^2 < 4V(E_p - E_0 + 2V)$ holds true, lowering in energy with N. For large enough N this inequality changes the sign, while the channel goes into the exponentially small transmission domain $E < E_0 - 2V$ (or $\varepsilon_0/2V > 1$) of the pristine AW.

Inside the pristine AW transmission band, close to the center of the band where $|\varepsilon_0/2V| \ll 1$, in Eq. (23) one has $\sin\phi = \sin[\arccos(\varepsilon_0/2V)] \approx \sin(\pi/2) = 1$ to within terms of the second order in $|\varepsilon_0/2V|$. Then, Eq. (23) becomes

$$\frac{d_N}{V^N} \approx \sin\left[\frac{(N+1)\pi}{2}\right] = \cos\left(\frac{N\pi}{2}\right) = i^N\,\frac{1+(-1)^N}{2}. \qquad (31)$$

Using this in Eqs. (17) and (18) to evaluate ρ_{N-1}, δ_N, δ_{N-1}, and δ_{N-2} in Eq. (29), one can simplify this equation to the form

$$T(E) \approx \frac{4\xi^2\left[\alpha_N(E) + \mu^2\sin(N\pi/2)\right]^2}{\left[(1+\xi^2)q\cos(N\pi/2+\eta) + (1-\xi^2)(-1)^N\mu^2\right]^2 + 4\xi^2\left[q\sin(N\pi/2+\eta) - (-1)^N\mu^2\right]^2}, \qquad (32)$$

where

$$\alpha_N(E) = \varepsilon_p(\varepsilon_0 + 2V) - N\mu^2 = (E - E_1)(E - E_2), \qquad (33)$$

$\eta = \arccos(\alpha_{N+1}/q)$, and $q = \sqrt{\alpha_{N+1}^2 + \mu^4}$. If $\mu = 0$, then Eqs. (31)–(33) bring us back to Eqs. (25) and (27) [with $\phi_k^{max(min)} = \pi/2$] for odd and even N, respectively. For non-zero μ the factor in the brackets in the numerator of Eq. (32) becomes either $\alpha_N^2(E)$ if N is even, or $\alpha_{N\mp1}^2(E)$ if N is odd of the form $4n \pm 1$, $n = 1, 2, 3, ...$ being positive integers. Then, in view of Eq. (33) and the fact that the denominator of Eq. (32) is always non-zero for $\mu \neq 0$, the transmission coefficient $T(E = E_2) = 0$ both in the former and in the latter case, for N and $N \mp 1$ respectively, once N is fixed. Thus, the E_2 energy level in the pristine AW transmission band blocks the transmission entirely, resulting in the *Fano resonance*, in full accord with the total resonant reflection effect of the standard Fano-Anderson model for a bound state within the continuum of scattering states[90,91]. The Fano resonance width Γ can be estimated from the focal parameter of the parabola one has in the numerator of Eq. (32) by setting $\alpha_{N,N\pm1} \approx \alpha_N \approx (E_2 - E_1)(E - E_2)$ for not too small N in the neighborhood of E_2 according to Eq. (33), whereas $\alpha_{N+1} \approx \alpha_N \approx 0$ in the denominator. As Eq. (32) is only valid in the neighborhood of E_0, there should be $E_2 \approx E_0$, and then $E_1 \approx E_p + 2V$ by Vieta's theorem, to result in

$$\Gamma \approx \frac{\mu^2\,\kappa(\xi, N)}{|E_0 - 2V - E_p|}, \qquad (34)$$

where

$$\kappa^2(\xi, N) = \left[\cos\left(\frac{N\pi}{2}\right) - (-1)^N\right]^2 + \frac{1}{4\xi^2}\left[(1+\xi^2)\sin\left(\frac{N\pi}{2}\right) - (1-\xi^2)(-1)^N\right]^2.$$

We see that the Fano resonance width is directly proportional to the square of the AW–CN coupling strength and varies strongly with N, while also being dependent on the relative position of the CN plasmon resonance energy and the pristine AW transmission band center. For $E_p \approx E_0 + 2V$, as it shows in Fig. 1 (c) in particular,

Eq. (34) results in $\Gamma \sim \mu^2/V$ in full accord with the standard Fano-Anderson model[91].

Outside of the pristine AW transmission band, in the domain of the exponentially small transmission where $|\varepsilon_0/2V| > 1$, Eq. (29) can be simplified by approximating the functions ρ_{N-1}, δ_N, δ_{N-1}, and δ_{N-2} with their respective leading terms in $|\varepsilon_0/2V|$, while keeping in mind that $\xi \ll 1$. This brings one to the following expression

$$T(E) \approx \frac{\xi^2 \mu^4}{\alpha_N^2(E)(\varepsilon_0/2V)^2 + [\alpha_N(E) + \mu^2]^2 \xi^2} \qquad (35)$$

to allow for evaluating various asymptotic regimes of the electron transfer through the additional plasmon-assisted transmission channels. One can see, in particular, that when $E = E_{1,2}$, whereby $\alpha_N = 0$, Eq. (35) yields the perfect transmission $T(E_{1,2}) = 1$. In the vicinity of the (more interesting) higher energy resonance transmission channel $E \approx E_1$ (and similar for $E \approx E_2$), Eq. (33) can be written as $\alpha_N \approx (E - E_1)(E_1 - E_2) \sim (E - E_1) 2\mu\sqrt{N}$, while $|\varepsilon_0| \approx |E_0 - E_1| \sim \mu\sqrt{N}$, for N large enough as can be seen from Eq. (30). This brings the transmission coefficient (35) to the form

$$T(E) \approx \frac{(\Delta/N)^2}{(E - E_1)^2 + (\Delta/N)^2}\,. \qquad (36)$$

We see the plasmon-assisted transmission energy channel to have the Lorentzian lineshape of the half-width-at-half-maximum Δ/N, that is proportional to the AW–lead coupling and inversely proportional to the AW length.

For energies far from $E_{1,2}$ resonances outside of the pristine AW transmission band, the function α_N in Eq. (33) is non-zero, allowing for two possible plasmon-mediated electron transmission regimes. If the AW is not too long, one can approximate $\alpha_N \approx \varepsilon_p(\varepsilon_0 + 2V)$ in Eq. (33). Then Eq. (35) takes the form

$$T(E) \approx \left[\frac{2\Delta\,\mu^2}{(E - E_p)(E - E_0)(E - E_0 - 2V)}\right]^2, \qquad (37)$$

in which $|(E - E_0)/2V| > 1$ and $E \neq E_p$. In this regime, the transmission coefficient shows no wire length dependence. For long enough AWs, one has $\alpha_N \approx -N\mu^2$, which being substituted into Eq. (35), results in

$$T(E) \approx \left(\frac{2\Delta}{E - E_0}\right)^2 \frac{1}{N^2}\,. \qquad (38)$$

This algebraic ($\sim N^{-2}$) transmission length dependence is much slower than the exponential transmission length dependence of Eq. (28) for pristine AWs. It comes from the slow plasmon-mediated transmission channel narrowing $\sim N^{-2}$ in Eq. (36). The inverse *quadratic* length dependence in Eq. (38) contrasts with the inverse *linear* length dependence of the phonon-mediated transmission typical of quasi-1D molecular wire systems[92].

V. NUMERICAL ANALYSIS

We assume that the leads and the AW are made of the same metal, and that the AW incapsulating carbon nanotube is end-bonded into the leads[93,94]. (Other possibilities for CN–lead contacts can be found in Ref.[95].) The equilibrium band lineup inside the hybrid AW–CN structure is then determined by the self-consistent charge redistribution through the entire metal-(CN–AW)-metal junction[94], to make $E_F = \epsilon_F$ and to position E_F of the entire system at equilibrium at the middle of the CN forbidden gap in the way it occurs for unpinned semiconducting CNs[93]. We analyze two representative semiconducting CNs to show two possibilities for relative arrangement of the CN interband plasmon resonance with respect to the encapsulated AW transmission band. They are the (11,0) CN and the (16,0) CN. With energy counted from the bottom of the CN fundamental bandgap $E_g^{(11)} = E_g$, by summing up the first bright exciton excitation and binding energies, 1.21 and 0.76 eV, as reported by Ma *et al.*[96] and Capaz *et al.*[97], respectively, one arrives at $E_g = 1.97$ eV for the (11,0) CN. This makes $E_0 = E_F = 0.985$ eV for the AW on-site energy and equilibrium Fermi energy of the complex hybrid system of the (11,0) CN encapsulating the AW of the same metal as that of leads. For the (16,0) CN, we evaluate $E_g = 1.47$ eV numerically using the $(\mathbf{k} \cdot \mathbf{p})$-method by Ando[18], to give $E_0 = E_F = 0.735$ eV for the AW encapsulating hybrid (16,0) CN system. For the AW, we use Na metal parameters, with the electron effective mass $m^* = 1.0\, m_0$[98] (m_0 is the free electron mass) and lattice constant $a = 4.225$ Å[99]. This yields the nearest neighbor electron hopping rate $V = \hbar^2/2m^*a^2 = 0.21$ eV. We choose the AW–lead coupling to be in the range $\Delta \sim 0.01 - 0.1$ eV as other authors earlier did[88,100]. The AW–CN coupling μ varies broadly in accordance with Eq. (11) as discussed at the beginning of Sec. IV.

Figure 1 (a), (b), (c) shows for the (11,0) and (16,0) CNs the real and imaginary parts of the low-energy conductivities as well as the real parts of the inverse conductivities and the local photonic DOS resonances originating from them, to scale with the finite-length (100 atoms) sodium AW transmission bands. To calculate the graphs in (a), we used the $(\mathbf{k} \cdot \mathbf{p})$-method by Ando with the exciton relaxation time 100 fs for both CNs (consistent with earlier estimates[101,102]). Many-particle Coulomb correlations are included in these calculations by solving the Bethe-Salpeter equation in the momentum space within the screened Hartree-Fock approximation as described in Ref.[18]. The real parts of the conductivities consist of series of peaks ($E_{11}, E_{22}, ...$) representing the 1st, 2nd, etc., excitons, and are linked with imaginary ones by the Kramers-Kronig relation. Therefore, the real parts of the inverse conductivities show the interband plasmon peaks $P_{11}, P_{22}, ...$ right next to $E_{11}, E_{22}, ...$ (first observed in Ref.[20]; see Refs.[22–28] for more details). The graphs in (b) show the local photonic DOS functions for the excited state non-radiative spontaneous decay of a two-level

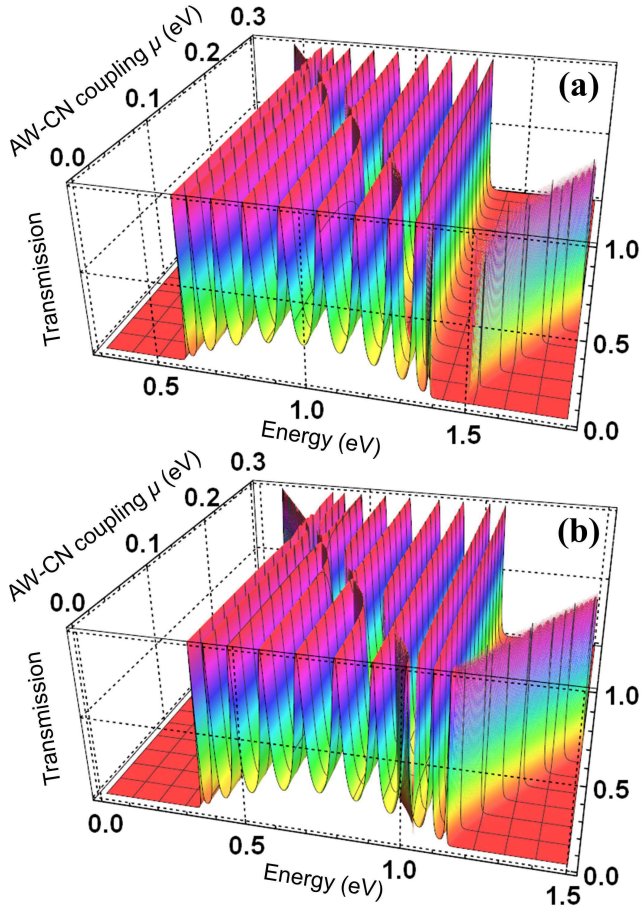

FIG. 2: (Color online) Transmission versus energy and AW-CN coupling strength as given by Eqs. (16)–(21) for the AW of length $N=10$ inside the (11,0) CN [$E_p \gtrsim E_F+2V$, panel (a)] and inside the (16,0) CN [$E_p \lesssim E_F+2V$, panel (b)]. AW-lead coupling constant $\Delta=0.05$ eV. [Cf. Fig. 1 (c)].

dipole emitter placed on the symmetry axis (inset) of the (11,0) and (16,0) CN. Details of these calculations and similar graphs for a variety of other geometry configurations can be found in Refs.[27–34]. Comparing (a) and (b), we see the sharp single-peak DOS resonances to come from the interband plasmons of respective CNs. These are responsible for the AW–CN near-field coupling in hybrid CN systems. The coupling is due to the virtual (vacuum-type) EM energy exchange between the AW and the CN to create and annihilate plasmons on the CN surface as described by the interaction Hamiltonian (10). Comparison with (c), which shows transmission bands for the 100 Na atoms chain calculated per Eqs. (22) and (23) with $\Delta=0.05$ eV to scale E_g for the (11,0) CN (top) and (16,0) CN (bottom), indicates that the 1st interband plasmon energy $E_p \sim E_F+2V$ and can be located both outside ($E_p \gtrsim E_F+2V$) and inside ($E_p \lesssim E_F+2V$) of the free AW electron transmission band.

These two possibilities are simulated and presented in Figure 2 (a) and (b). Here, we show the transmission as given by Eqs. (16)–(21) for the AW of 10 sodium atoms in length inside the (11,0) CN [(a), $E_p \gtrsim E_F+2V$] and inside the (16,0) CN [(b), $E_p \lesssim E_F+2V$] under the AW–lead coupling $\Delta=0.05$ eV with the AW–CN coupling μ varied from 0 up to 0.3 eV over the energy range to cover the entire free AW transmission band [cf. Fig. 1 (c)]. At zero μ, in accordance with Eqs. (25) and (27), we see the free AW transmission band of 10 resonance electron transfer channels $T^{max}_{k=\overline{1,10}} \approx 1$ separated by the transmission minima $T^{min}_{k=\overline{1,9}}$ that are controlled by the magnitude of Δ as discussed following Eq. (27). As μ departs from zero to increase, the near-field AW–CN interaction is seen to block some of the electron transfer channels in the AW transmission band, while opening up extra (plasmon-induced) electron transfer channels in the CN forbidden gap outside of the AW transmission band. Depending on whether E_p is outside or inside of the AW transmission band, the higher energy plasmon-induced transfer channel in the CN forbidden gap either shows up gradually [panel (a)], or splits off from the top of the free AW transmission band [panel (b)]. The exact energies of the emerging and blocked transmission channels are given by $E_{1,2}$ in Eq. (30), and their behavior is in agreement with that discussed in the previous section.

Figure 3 (a), (b), (c), and (d) illustrates in detail the Fano resonance effect discussed in the previous section. We see the transmission versus energy calculated according to Eqs. (16)–(21) for the sodium AW of varied length $N=100$, 101, 102, and 103 inside the (11,0) CN under the AW–CN coupling $\mu=0.045$ eV and the AW–lead coupling $\Delta=0.1$ eV. Dashed and dotted vertical lines trace the band gap ($E_g=1.97$ eV) and the first interband plasmon energy ($E_p=1.50$ eV) for the (11,0) CN (cf. Fig. 1). Red thick dashed lines show the approximate transmission curves given by Eq. (32) valid in the neighborhood of the AW transmission band center (hence the choice of μ and Δ in this calculation). Green lines are the parabolas of Eq. (33). They are seen to intersect the abscise axis at two points, $E=E_{1,2}$ given by Eq. (30). At $E=E_2$ inside the AW band, the transmission drops down to zero in view of the fact that this coupled AW–CN state (which can also be interpreted as one of the *two* branches to represent the "dressed" states of the mixed CN plasmon and AW electron excitations[32,33]) is not a well defined eigen state of the entire hybrid system. An electron can occupy this state just temporarily, not permanently, as there is always a high probability for it to leave for one of the many band states that are available in this energy domain. That is why this coupled AW–CN state behaves as a scattering resonance to reflect an incident electron flux at $E=E_2$, thereby blocking the transmission at this energy. Another coupled AW–CN state, the second branch of the mixed CN plasmon and AW electron excitations, is isolated at $E=E_1$ in the CN forbidden gap outside the AW band. This is a well defined eigen state of the hybrid AW–CN system, which opens up a new plasmon-mediated resonance transmission channel.

Figure 4 shows the transmission as a function of the AW length, calculated from Eqs. (16)–(21) for the AW

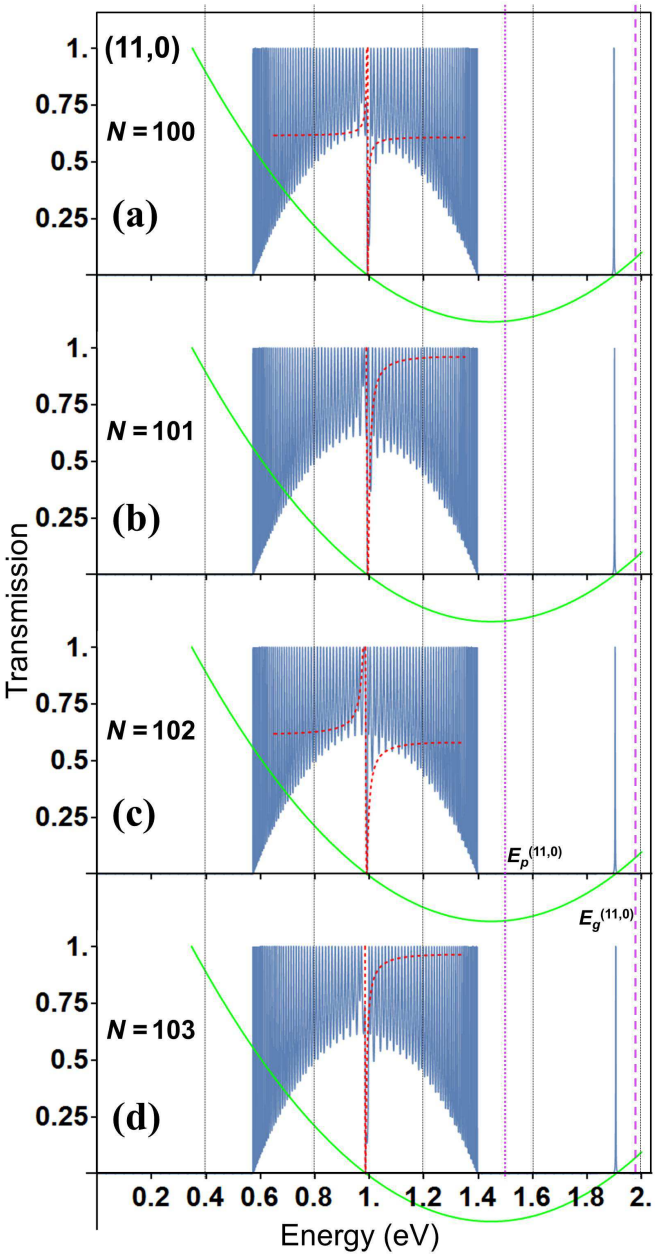

FIG. 3: (Color online) Transmission versus energy as given by Eqs. (16)–(21) for the AW of varying length $N = 100-103$ [(a)–(d)] inside the (11,0) CN. AW-CN and AW-lead coupling constants are $\mu = 0.045$ eV and $\Delta = 0.1$ eV, respectively. Red dashed lines are zone-center approximations of Eq. (32). Green lines are parabolas of Eq. (33). [Cf. Fig. 1 (c)].

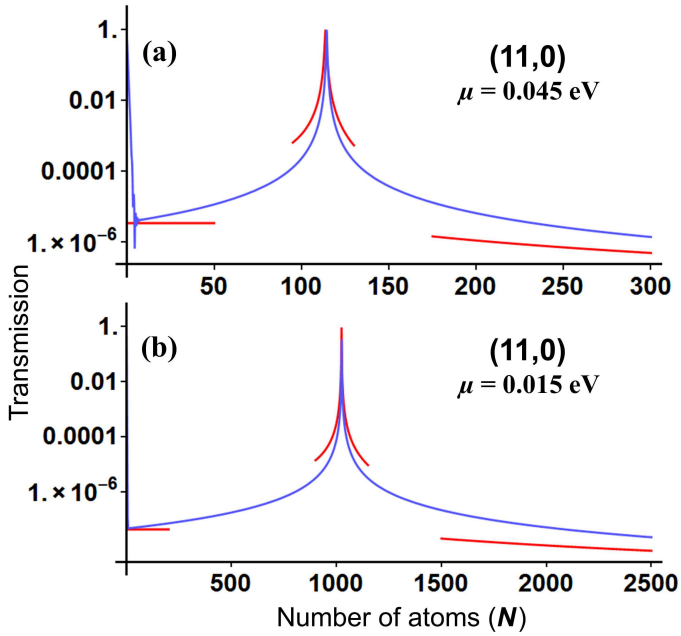

FIG. 4: (Color online) Log-scaled transmission versus the AW length as given by Eqs. (16)–(21) for the AW inside the (11,0) CN at $E = 1.93$ eV (CN forbidden gap outside of the AW transmission band, cf. Fig. 3). AW–CN coupling $\mu = 0.045$ eV in (a) and 0.015 eV in (b), AW–lead coupling $\Delta = 0.1$ eV. Red lines are the near-resonance and short/long-AW out-of-resonance approximations of Eqs. (36) (middle line), (37) (left line) and (38) (right line), respectively.

inside the (11,0) CN. The energy is fixed at $E = 1.93$ eV, that is inside the CN forbidden gap but outside the pristine AW transmission band, and is close to the plasmon-mediated resonance transmission channel E_1 in Fig. 3. Red lines indicate the approximations given by Eq. (36) in the neighborhood of E_1 (middle line), and by Eqs. (37) and (38) away from E_1 in the short AW (left line) and long AW (right line) limits. In (a) the same coupling parameters as in Fig. 3 are used, while in (b) the AW–CN coupling is reduced by a factor of three. We see that the resonance plasmon-mediated transmission depends strongly on the AW–CN coupling strength μ, and can be achieved both at shorter and at longer AW length for stronger and weaker coupling, respectively. The energy of the plasmon-mediated transmission channels is controlled by the product $N\mu^2$ as given by Eq. (30). Therefore, to reach the resonance transmission regime of Eq. (36) at fixed energy E with μ reduced by a factor of three, one has to increase N by a factor of nine. That is exactly what we see comparing (a) and (b) in Fig. 4. This peculiarity is the key to practical applications of the plasmon-mediated coherent resonance transmission phenomenon.

It is interesting to see how the AW–CN coupling affects the transmission at the Fermi level energy $E = E_F$. For pristine monoatomic wires of finite length it is known, in particular, that depending on the valence and interatomic spacing their conductance shows both odd-even atom number oscillations and more complicated features such as four-atom and six-atom period oscillations (see Refs.[103–107] and refs. therein for details]. Figure 5 shows the transmission coefficient versus the AW length calculated from Eqs. (16)–(21) for the AW inside the (11,0) CN at $E = E_F = 0.985$ eV. The graphs for the AW–(16,0) CN system look similar, and so are not shown here. In (a) and (b) the AW–CN coupling $\mu = 0$ and 0.15 eV, respectively, while $\Delta = 0.05$ eV as in Fig. 2 (a). In (c)

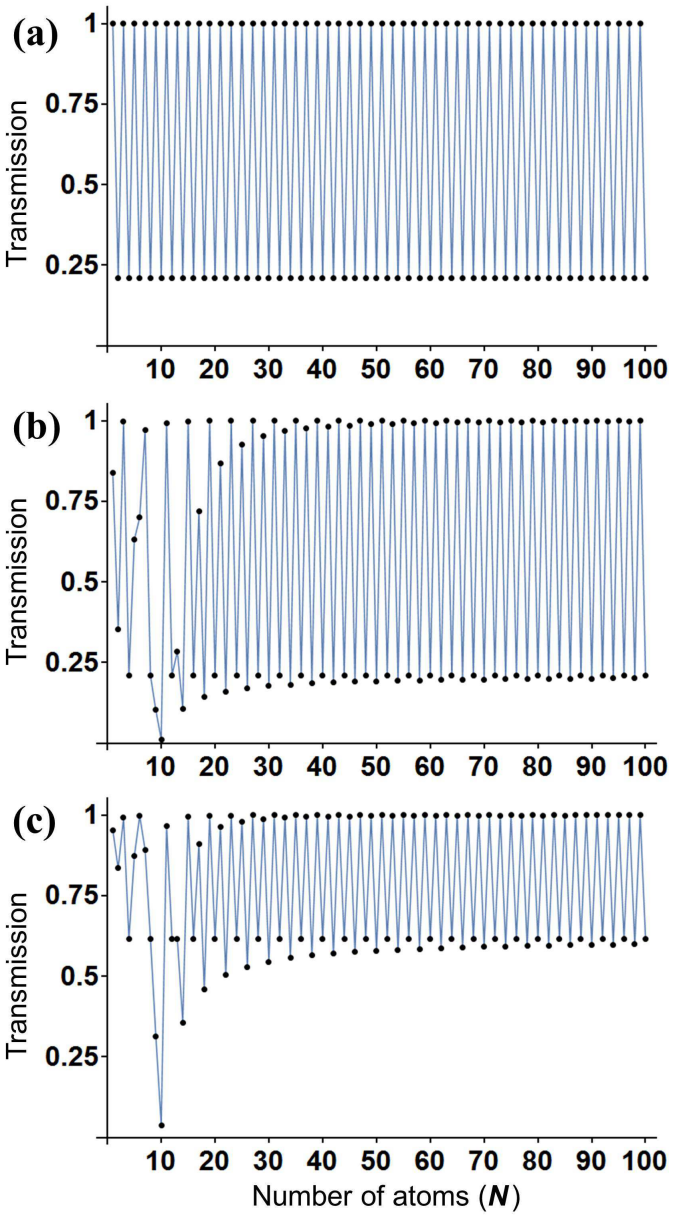

FIG. 5: (Color online) Transmission versus the AW length as given by Eqs. (16)–(21) for the AW inside the (11,0) CN at $E = E_F = 0.985$ eV [cf. Fig. 2 (a)]. Panel (a): $\mu = 0$ eV, $\Delta = 0.05$ eV. Panel (b): $\mu = 0.15$ eV, $\Delta = 0.05$ eV. Panel (c): $\mu = 0.15$ eV, $\Delta = 0.1$ eV.

the AW–lead coupling is increased by a factor of two, $\Delta = 0.1$ eV, while $\mu = 0.15$ eV is the same as in (b). The odd-even atom number oscillations of the pristine AW in panel (a) come from the oscillatory behavior of d_N in Eq. (23) at $\varepsilon_0 = 0$, whereby d_N is zero or non-zero to yield maximal or minimal transmission in Eq. (22) for odd or even N, respectively. In panels (b) and (c), where the AW–CN coupling is non-zero, the distinct behavior can be understood from Eq. (32), which is the *exact* representation of Eq. (29) for $E = E_0 = E_F$. With $\xi^2 \ll 1$, this equation is seen to have maxima when

$$q \cos\left(\frac{N\pi}{2} + \eta\right) + (-1)^N \mu^2 = 0, \tag{39}$$

where $\eta = \arccos(\alpha_{N+1}/q)$ and $q = \sqrt{\alpha_{N+1}^2 + \mu^4}$ with $\alpha_N = 2V(E_p - E_F) - N\mu^2$. The case where $\alpha_{N+1} = 0$ was discussed in the previous section. The transmission coefficient experiences the Fano resonance at $E = E_F$ then. This can be clearly seen in panels (b) and (c) for $N = 10$ [and also in Fig. 2 (a)] for the parameters chosen. For non-zero α_{N+1} such that $\alpha_{N+1}^2 \ll \mu^4$, that is for N given by the inequality $|N + 1 - 2V(E_p - E_F)/\mu^2| \ll 1$, one has $q \approx \mu^2$ and $\eta \approx \pi/2$. Then Eq. (39) fulfils for all integer n such that $N = 4n + 3$, yielding four-atom periodic transmission maxima one can see at low and moderate N in panels (b) and (c). As N increases and becomes large enough, one necessarily obtains $\alpha_{N+1}^2 \approx \alpha_N^2 \gg \mu^4$, to yield $q \approx |\alpha_N| \approx N\mu^2$ and $\eta \approx \pi$. As this takes place, Eq. (39) takes the form $\cos(N\pi/2) = (-1)^N/N \approx 0$ while the μ dependence in Eq. (32) cancels, resulting in odd-even atom number transmission oscillations that are only dependent on the AW–lead coupling Δ as one can see from the graphs in panels (b) and (c).

VI. DISCUSSION

In this study, we consider coherent electron transport through the one-atom-thick, finite-length metallic wire encapsulated in a semiconducting CN whose forbidden gap is broader than the conduction band of the wire. To obtain tractable theoretical results of relevance to the experimental situation, this hybrid metal-semiconductor CN system is assumed to be connected to the leads of the same metal as the wire itself. We ignore a variety of incoherent electron scattering processes such as those that are typical and normally studied for complex *molecular* junction systems, including vibronic coupling[92,108], coupling to defects[109], particularities of the coupling to the leads[100,110], etc.[111] Discussion of all these processes would take us far away from the main topic of our work, which is to understand the inter-play between the intrinsic 1D conductance of metallic AWs and the CN mediated near-field effects in hybrid metal-semiconductor nanotube systems. In our hybrid systems, incoherent processes like this also include electron exchange between the wire and the nanotube, which we do not expect to be significant due to rather strong ionization potentials of atomic metals ~ 5 eV and their moderate electronegativity relative to carbon ($\sim 0.3 - 1.8 < 2$)[112], that is insufficient to pull electrons of metal over to carbon. Overall, incoherent effects can be quite generally accounted for in our model by introducing a phenomenological finite plasmon lifetime. This redefines E_p to $E_p - i\Delta E_p$ with the imaginary part representing the half-width (inverse lifetime) of the plasmon resonance, which is equivalent

to the replacement

$$\delta(\omega - E_p/\hbar) \longrightarrow \frac{1}{\pi}\frac{\Delta E_p/\hbar}{(\omega - E_p/\hbar)^2 + (\Delta E_p/\hbar)^2}$$

in Eq. (9) above. Substitution of thus modified Eq. (9) into the CN Hamiltonian (8) does not make any change to it provided that $\Delta E_p \ll E_p$, in which case the plasmon resonance is sharp and plasmons are well-defined long-lived excitations of the nanotube, whereby

$$\int_0^\infty \frac{d\omega\, \hbar\omega\, \Delta E_p/(\pi\hbar)}{(\omega - E_p/\hbar)^2 + (\Delta E_p/\hbar)^2}$$

$$\approx E_p \int_0^\infty \frac{d\omega\, \Delta E_p/(\pi\hbar)}{(\omega - E_p/\hbar)^2 + (\Delta E_p/\hbar)^2}$$

$$= \frac{E_p}{\pi}\left[\arctan\left(\frac{E_p}{\Delta E_p}\right) + \frac{\pi}{2}\right] \approx E_p,$$

thus leaving our results unchanged up to terms of the first non-vanishing order in $\Delta E_p/E_p$.

In our approach, the AW is treated within the single-hopping-parameter (or single-band) tight-binding model. Such a model is realistic for the 1D chains of atoms with half-filled outermost s-shells. These include monovalent alkali metals and transition metals with filled d- (and f-) shells such as copper, silver, and gold. The single atom $|s\rangle$- and $|p\rangle$-states of the same principal quantum number combine, due to their quasi-degeneracy, to form an ordinary conduction band of mixed parity[113]. Such bands allow for a *non-zero* electron transition dipole moment $d_z \sim \langle s|\hat{d}_z|p\rangle$ to control the AW–CN dipole coupling constant μ in Eqs. (10) and (11). Other transition metals would feature multi-band (multi-channel[106]) conductance due to their under-filled d- (and f-) shells. However when allowed by parity, the AW–CN near-field interaction (10) is universal in its nature, and is hardly sensitive to conductance peculiarities for them to be able to affect our results.

Our main result is the prediction of the sharp Fano resonances in the electron transmission through the hybrid quasi-1D nanostructures of semiconducting CNs that encapsulate metal AWs. The resonances are due to the AW–CN near-field interaction given by Eqs. (10) and (11). The interaction couples the AW electron and CN plasmon excitations to form two branches of the mixed ("dressed"[32,33]) states to represent the eigen states of the entire hybrid system. The quantity that controls the coupling is $N\mu^2$ in Eq. (30). Therefore, regardless of how E_p and E_F are positioned relative to each other in the CN forbidden gap, a significant AW–CN coupling strength can be achieved in structures of varied length even if the single-atom coupling constant μ is small. Quite generally, the condition for the conductance $g = T(E \sim E_F = \epsilon_F)$ of the hybrid metal-semiconductor CN structure to be affected significantly by the AW–CN plasmon coupling can be formulated as $\alpha_N(E_F) = 0$ with $\alpha_N(E)$ out of Eq. (33). This translates into regular notations to give

$$2V(E_p - E_F) = N\mu^2. \tag{40}$$

If, for certain μ and N, this equation is fulfilled, then a coupled AW–CN state falls right at the middle of the AW transmission band (E_2 in Figs. 2 and 3). Such a "Fano" state, being closely surrounded by the band states, ceases to be the well-defined eigen state of the hybrid system. It turns into the scattering resonance to reflect an incident electron flux and thus to block the conductance [as it shows in Fig. 5 (b) and (c)]. At the same time, with Eq. (40) fulfilled, the second coupled AW–CN plasmon state emerges outside of the AW band at $E = E_p + 2V$. If it happens to be isolated inside of the CN forbidden gap (like E_1 in Figs. 2 and 3), then this second "Fano" state presents a well-defined eigen state of the hybrid system to open up a new plasmon-mediated coherent transmission channel in the energy domain where neither of the individual pristine constituents, neither AW nor CN, is transparent. The transport through this channel can be quite efficient even if the coupling constant μ, the AW length N, and the transmission energy are out of their resonance values since the out-of-resonance transmission coefficient falls down with N relatively slowly, $\sim 1/N^2$, as one can see from Eq. (38) shown in Fig. 4.

The features described of the Fano resonances we predict are quite generic. They originate from the similarity between our model Hamiltonian (5)–(11) and the general Fano-Anderson model for a bound quantum state inside or outside of the continuum of scattering states[90]. Therefore, the Fano resonances can also manifest themselves in those metal-nanotube combinations where the AW transmission band happens to be broader than the CN forbidden gap. They may affect electron transport in the CN conduction band as well as hole transport in the CN valence band, since E_1 enters the CN conduction band and E_2 enters the CN valence band at large $N\mu^2$ (Fig. 2). The result will be transmission reduction for some of the channels inside of a band of states and/or an extra plasmon-mediated coherent transmission resonance in the energy domain where no band states are available.

In our model, the single-atom AW–CN coupling constant μ in Eq. (11) is considered to be site independent. In reality, the structure of the AWs encapsulated in the nanotube can be quite different from that of pristine AWs due to factors such as atom clustering[71], dimerization[75], multiple atomic chains formation[54], as well as a variety of random spontaneous deformations of atomic chains inside the CN. In all these and other related cases, our model coupling constant μ should be considered as the effective mean interaction constant. Local deviations from the mean value due to the factors mentioned will definitely cause the inhomogeneous broadening of the Fano resonances we predict — both inside of the AW transmission band to increase the Γ estimate in Eq. (34), in particular, and outside of the AW band to broaden the plasmon-mediated coherent transmission channel in the CN forbidden gap (see Figs. 2 and 3).

Overall, by selectively controlling the AW length N in the process of sample fabrication[106], one might be able, in principle, to manipulate by the electron trans-

port regimes as it shows in Figs. 4 and 5 and is commented above — both inside and outside of the CN forbidden gap, both to reduce and to enhance the transmission of the hybrid AW–CN system. Controlling the AW length can also be supplemented with other external means, such as the AW transmission band tune-up through chemical or electrostatic gate control[114,115], electrostatic doping to adjust the CN forbidden gap[116], and the quantum confined Stark effect to tune the CN plasmon energy[24], thus allowing for flexible transport optimization in hybrid metal-semiconductor CN systems in ways desired for practical applications.

VII. CONCLUSIONS

We study coherent electron transport through the one-atom-thick, finite-length metallic wire encapsulated into a semiconducting carbon nanotube with the forbidden gap broader than the AW conduction band. We use the matrix Green's functions formalism to develop the electron transfer theory for such a hybrid metal-semiconductor system. Our goal is to understand the inter-play between the intrinsic 1D conductance of the atomic wire and nanotube mediated near-field effects.

The theory we developed predicts the Fano resonances in electron transmission through the system. That is the AW–CN near-field interaction blocks some of the pristine AW transmission band channels to open up new coherent channels in the CN forbidden gap outside the AW transmission band. This makes the entire hybrid system transparent in the energy domain where neither AW nor CN is individually transparent. These generic features of the Fano resonances we predict may also manifest themselves in those metal-nanotube combinations where the AW transmission band is broader than the CN forbidden gap. They may affect both electron transport in the CN conduction band and hole transport in the CN valence band to block some of the transmission channels inside and/or to provide extra plasmon-mediated coherent transmission channels outside of bands of states. This effect can be used to control and optimize charge transfer in hybrid metal-semiconductor CN based devices for nanoscale energy conversion, separation, and storage.

VIII. ACKNOWLEDGMENTS

M.F.G. is supported by Deutsche Forschungsgemeinschaft through the Cluster of Excellence "Munich-Centre for Advanced Photonics" (www.munich-photonics.de). M.F.G. acknowledges the hospitality of the Department of Mathematics and Physics at North Carolina Central University, USA, where this work was started during the visit sponsored by the US NSF (ECCS-1306871). I.V.B. is supported by DOE (DE-SC0007117).

Appendix A: Derivation of equations (17) and (18)

Using the matrix $\mathbf{H}$ in Eq. (12), one can derive the recursion relations for the quantities D_N and S_N to determine $T(E)$ in Eqs. (16) and (29).

Recursion relation for D_N.

Expanding the determinant $D_N = \det(\mathbf{H} - E)$ along the first row, one has the set of recursion relations as follows

$$D_N = \varepsilon_0 D_{N-1} - V A_N + (-1)^N \mu F_N, \quad \text{(A1)}$$

$$A_N = V D_{N-2} - (-1)^N \mu F_{N-1}, \quad \text{(A2)}$$

$$F_N = V F_{N-1} - (-1)^N \mu d_{N-1}, \quad \text{(A3)}$$

$$d_N = \varepsilon_0 d_{N-1} - V^2 d_{N-2}, \quad \text{(A4)}$$

where A_N, F_N, and d_N are the determinants of the $N\times N$ matrixes

$$\mathbf{A} = \begin{bmatrix} V & V & 0 & \dots & 0 & 0 & \mu \\ 0 & \varepsilon_0 & V & \dots & 0 & 0 & \mu \\ 0 & V & \varepsilon_0 & \dots & 0 & 0 & \mu \\ \vdots & \vdots & \vdots & \ddots & \vdots & \vdots & \vdots \\ 0 & 0 & 0 & \dots & \varepsilon_0 & V & \mu \\ 0 & 0 & 0 & \dots & V & \varepsilon_0 & \mu \\ \mu & \mu & \mu & \dots & \mu & \mu & \varepsilon_p \end{bmatrix},$$

$$\mathbf{F} = \begin{bmatrix} V & \varepsilon_0 & V & 0 & \dots & 0 & 0 \\ 0 & V & \varepsilon_0 & V & \dots & 0 & 0 \\ 0 & 0 & V & \varepsilon_0 & \dots & 0 & 0 \\ \vdots & \vdots & \vdots & \ddots & \ddots & \vdots & \vdots \\ 0 & 0 & \dots & 0 & V & \varepsilon_0 & V \\ 0 & 0 & \dots & 0 & 0 & V & \varepsilon_0 \\ \mu & \mu & \dots & \mu & \mu & \mu & \mu \end{bmatrix},$$

and

$$\mathbf{d} = \begin{bmatrix} \varepsilon_0 & V & 0 & \dots & 0 & 0 & 0 \\ V & \varepsilon_0 & V & \dots & 0 & 0 & 0 \\ 0 & V & \varepsilon_0 & \dots & 0 & 0 & 0 \\ \vdots & \vdots & \vdots & \ddots & \vdots & \vdots & \vdots \\ 0 & 0 & 0 & \dots & \varepsilon_0 & V & 0 \\ 0 & 0 & 0 & \dots & V & \varepsilon_0 & V \\ 0 & 0 & 0 & \dots & 0 & V & \varepsilon_0 \end{bmatrix},$$

respectively. Using Eqs. (A2) and (A3) to eliminate A_N in Eq. (A1) results in

$$D_{N+2} - \varepsilon_0 D_{N+1} + V^2 D_N = 2(-1)^N \mu V F_{N+1} - \mu^2 d_{N+1}, \quad \text{(A5)}$$

This is the recursion relation for D_N. It should be solved together with recursion relations (A3) and (A4) under the initial conditions as follows

$$D_0 = \varepsilon_p, \quad D_1 = \varepsilon_0 \varepsilon_p - \mu^2;$$
$$F_0 = 0, \quad F_1 = \mu; \qquad d_0 = 1, \quad d_1 = \varepsilon_0. \quad \text{(A6)}$$

Recursion relation for S_N.

According to Eqs. (13)–(15), the quantity S_{N-1} of interest is the $N1$ minor of the matrix $\mathbf{H}-E$. This is given by the determinant of the $N\times N$ matrix

$$\mathbf{S}=\begin{bmatrix} V & 0 & 0 & 0 & \dots & 0 & \mu \\ \varepsilon_0 & V & 0 & 0 & \dots & 0 & \mu \\ V & \varepsilon_0 & V & 0 & \dots & 0 & \mu \\ \vdots & \ddots & \ddots & \ddots & \vdots & \vdots & \vdots \\ 0 & \dots & V & \varepsilon_0 & V & 0 & \mu \\ 0 & \dots & 0 & V & \varepsilon_0 & V & \mu \\ \mu & \dots & \mu & \mu & \mu & \mu & \varepsilon_p \end{bmatrix}.$$

Expanding $S_{N-1}=\det(\mathbf{S})$ along the first row, one has

$$S_{N-1} = VS_{N-2}-(-1)^N\mu\, B_{N-2}, \tag{A7}$$

$$B_{N-1} = \mu\, d_{N-2}-VB_{N-2}, \tag{A8}$$

where B_{N-1} is the determinant of the $N\times N$ matrix

$$\mathbf{B}=\begin{bmatrix} \varepsilon_0 & V & 0 & \dots & 0 & 0 & 0 \\ V & \varepsilon_0 & V & \dots & 0 & 0 & 0 \\ 0 & V & \varepsilon_0 & \dots & 0 & 0 & 0 \\ \vdots & \vdots & \vdots & \ddots & \vdots & \vdots & \vdots \\ 0 & 0 & 0 & \dots & \varepsilon_0 & V & 0 \\ 0 & 0 & 0 & \dots & V & \varepsilon_0 & V \\ \mu & \mu & \mu & \dots & \mu & \mu & \mu \end{bmatrix}.$$

Combining Eqs. (A7) and (A8), one arrives at the recursion relation as follows

$$S_{N+2}-2VS_{N+1}+V^2S_N=(-1)^N\mu^2 d_N, \tag{A9}$$

to be solved under the initial conditions

$$S_0=\varepsilon_p,\quad S_1=V\varepsilon_p-\mu^2;$$
$$d_0=\varepsilon_0,\quad d_1=\varepsilon_0^2-V^2. \tag{A10}$$

The d_N initial condition is now one element downshifted [cf. Eq. (A6)] to reflect the fact of the dimensionality reduction in Eq. (A9) compared to Eq. (A5).

Solving recursion relations (A5) and (A9).

Recursion relations (A5) and (A9) are a convenient set of the recursion formulas for the numerical evaluation of the transmission coefficient in Eq. (16). They allow for the exact solution though, and so will be solved here analytically. According to Ref.[117], the solution to the second order constant coefficient inhomogeneous recursive relation

$$y_{N+2}+a\,y_{N+1}+b\,y_N=f_N \tag{A11}$$

(a and b are constant coefficients, f_N is a known function) is given by the expression as follows

$$y_N=y_1\zeta_{N-1}-y_0 b\,\zeta_{N-2}+\sum_{k=0}^{N-2} f_k\zeta_{N-k-2}. \tag{A12}$$

Here

$$\zeta_N=\frac{\lambda_1^{N+1}-\lambda_2^{N+1}}{\lambda_1-\lambda_2} \tag{A13}$$

with $\lambda_{1,2}$ being the roots of the characteristic equation $\lambda^2+a\,\lambda+b=0$. For $\lambda_1=\lambda_2$, Eq. (A13) takes the form

$$\zeta_N=(N+1)\,\lambda_1^N. \tag{A14}$$

Starting with Eq. (A4) and bringing it to the standard form (A11), one has

$$d_{N+2}-\varepsilon_0\, d_{N+1}+V^2 d_N=0.$$

This is to be solved with initial conditions (A6) and (A10) for recursion relations (A5) and (A9), respectively. Using Eq. (A11) with $f_N=0$, Eq. (A12) and Eq. (A13), one obtains Eq. (20) under initial conditions (A6), and

$$d_N=\frac{\lambda_1^{N+2}-\lambda_2^{N+2}}{\lambda_1-\lambda_2} \tag{A15}$$

under initial conditions (A10), where $\lambda_{1,2}$ are the roots of the characteristic equation $\lambda^2-\varepsilon_0\lambda+V^2=0$. They are given by Eq. (21), and are subject to Vieta's formulas whereby $\lambda_1+\lambda_2=\varepsilon_0$ and $\lambda_1\lambda_2=V^2$.

Similarly, bringing Eq. (A3) to the form (A11), one has

$$F_{N+2}-VF_{N+1}=-(-1)^N\mu\, d_{N+1},$$

which should be solved under initial conditions (A6). Then, Eq. (A12) with $f_N=-(-1)^N\mu\, d_{N+1}$, where d_N is given by Eq. (20), results in

$$F_N=\mu\, V^{N-1}-\mu\sum_{k=0}^{N-2\,(\geq 0)}(-1)^k\,\frac{\lambda_1^{k+2}-\lambda_2^{k+2}}{\lambda_1-\lambda_2}\,V^{N-k-2}.$$

Here, the second term can be found by summing up two geometric series with common ratios $-\lambda_1/V$ and $-\lambda_2/V$, respectively, to result in the final expression as follows

$$F_N=\frac{\mu}{\varepsilon_0+2V}\left[V^N-(-1)^N(d_N+Vd_{N-1})\right]. \tag{A16}$$

With F_N determined by Eqs. (A16), the right hand side of Eq. (A5) becomes

$$q_N=\frac{\mu^2}{\varepsilon_0+2V}\left\{2V^2\left[d_N+(-1)^N V^N\right]-\varepsilon_0 d_{N+1}\right\}.$$

This can be further rewritten as

$$q_N=\frac{\mu^2}{\varepsilon_0+2V}\left[2(-1)^N V^{N+2}-\lambda_1^{N+2}-\lambda_2^{N+2}\right] \tag{A17}$$

using Eq. (A4) followed by Eq. (20) to express d_{N+2} and d_N in terms of $\lambda_{1,2}$. With $f_N=q_N$ of Eq. (A17) and $\zeta_N=d_N$, Eqs. (A11)–(A13) under initial conditions (A6) result in the solution to Eq. (A5) as follows

$$D_N=\left(\varepsilon_0\varepsilon_p-\mu^2\right)d_{N-1}-\varepsilon_p V^2 d_{N-2}$$
$$+\sum_{k=0}^{N-2\,(\geq 0)} q_k d_{N-k-2}. \tag{A18}$$

Here, the first two terms can be written as $\varepsilon_p d_N - \mu^2 d_{N-1}$ in view of Eq. (A4). The third term can be evaluated by summing up the geometric series in the same way as it was done to derive Eq. (A16). There are three contributions to the total sum that originate from the three terms in Eq. (A17). Using Eqs. (20) and (A4) as well as the fact that $\lambda_1 + \lambda_2 = \varepsilon_0$ and $\lambda_1\lambda_2 = V^2$, one has

$$\sum_{k=0}^{N-2\,(\geq 0)} (-1)^k V^{k+2} d_{N-k-2} = V d_{N-1} + \frac{V}{\varepsilon_0 + 2V}\left[(-1)^N V^N - V d_{N-1} - d_N\right]$$

and

$$\sum_{k=0}^{N-2\,(\geq 0)} \lambda_1^{k+2} d_{N-k-2} + \sum_{k=0}^{N-2\,(\geq 0)} \lambda_2^{k+2} d_{N-k-2} = N d_N - \varepsilon_0 d_{N-1},$$

to result in

$$\sum_{k=0}^{N-2\,(\geq 0)} q_k d_{N-k-2} = \mu^2 d_{N-1} + \frac{\mu^2}{\varepsilon_0 + 2V}\left\{-N d_N + \frac{2V}{\varepsilon_0 + 2V}\left[(-1)^N V^N - V d_{N-1} - d_N\right]\right\}$$

after elementary algebraic simplifications. Substituting this into the right hand side of Eq. (A18), one finally arrives at Eq. (17).

Equation (A9) must be solved with d_N of Eq. (A15) consistent with the initial conditions (A10), as opposed to Eq. (A5) where d_N on the right is given by Eq. (20). Following Eqs. (A11) and (A12) with $\zeta_N = (N+1)V^N$, one then obtains the solution of the form

$$S_N = \varepsilon_p V^N - \mu^2 N V^{N-1} + \mu^2 \sum_{k=0}^{N-2\,(\geq 0)} (-1)^k \frac{\lambda_1^{k+2} - \lambda_2^{k+2}}{\lambda_1 - \lambda_2} (N-k-1) V^{N-k-2}. \tag{A19}$$

Here, the sum over k can be done by rewriting it as

$$\frac{\partial}{\partial V} \sum_{k=0}^{N-2\,(\geq 0)} (-1)^k \frac{\lambda_1^{k+2} - \lambda_2^{k+2}}{\lambda_1 - \lambda_2} V^{N-k-1},$$

followed by summing up the geometric series, differentiation, and algebraic simplifications subject to $\lambda_1 + \lambda_2 = \varepsilon_0$ and $\lambda_1\lambda_2 = V^2$, to result in the expression as follows

$$\frac{\lambda_1 - \lambda_2}{\varepsilon_0 + 2V}\left[(N-1)V^N + \varepsilon_0 N V^{N-1} + (-1)^N \frac{\lambda_1^{N+1} - \lambda_1^{N+1}}{\lambda_1 - \lambda_2}\right].$$

Substituting this into the right hand side of Eq. (A19), after simplifications one finally arrives at Eq. (18).

* Corresponding author: ibondarev@nccu.edu

[1] N.Agrait, A.L.Yeyati, J.M.van Ruitenbeek, Phys. Rep. **377**, 81 (2003).
[2] S.Datta, Nanotechn. **15**, S433 (2004).
[3] A.Nitzan and M.Ratner, Science **300**, 1384 (2003).
[4] N.A.Zimbovskaya and M.R.Pederson, Phys. Rep. **509**, 1 (2011).
[5] J.-C.Charlier, X.Blase, and S.Roche, Rev. Mod. Phys. **79**, 677 (2007).
[6] R.Saito, G.Dresselhaus, and M.S.Dresselhaus, *Science of Fullerens and Carbon Nanotubes* (Imperial College, London, 1998).
[7] M.Dresselhaus, G.Dresselhaus, and Ph.Avouris (eds.), *Carbon Nanotubes: Synthesis, Structure, Properties, and Applications* (Springer-Verlag, Berlin, 2001).
[8] M.F.L.De Volder, S.H.Tawfick, R.H.Baughman, and A.J.Hart, Science **339**, 535 (2013).
[9] Ph.Avouris, M.Freitag, and V.Perebeinos, Nature Photon. **2**, 341 (2008).
[10] F.Vietmeyer, B.Seger, and P.V.Kamat, Adv. Mater. **19**, 2935 (2007).
[11] N.M.Gabor, Z.Zhong, K.Bosnick, J.Park, and P.L.McEuen, Science **325**, 1367 (2009).
[12] T.Mueller, M.Kinoshita, M.Steiner, V.Perebeinos, A.A.Bol, D.B.Farmer, and Ph.Avouris, Nature Nanotechn. **5**, 27 (2010).
[13] T.Hertel, Nature Photon. **4**, 77 (2010).
[14] X.Dang, H.Yi, M.-H.Ham, J.Qi, D.S.Yun, R.Ladewski, M.S.Strano, P.T.Hammond, and A.M.Belcher, Nature Nanotechn. **6**, 377 (2011).
[15] E.Malic, C.Weber, M.Richter, V.Atalla, T.Klamroth, P.Saalfrank, S.Reich, and A.Knorr, Phys. Rev. Lett. **106**, 097401 (2011).
[16] S.Nanot, E.H.Haroz, J.-H.Kim, R.H.Hauge, and J.Kono, Adv. Mater. **24**, 4977 (2012).
[17] T.Hertel and I.V.Bondarev, eds., *Photophysics of Carbon Nanotubes and Nanotube Composites* (Special Issue), Chem. Phys. **413**, 1–131 (2013).
[18] T.Ando, J. Phys. Soc. Jpn. **74**, 777–817 (2005).
[19] M.S.Dresselhaus, G.Dresselhaus, R.Saito, and A.Jorio, Annu. Rev. Phys. Chem. **58**, 719 (2007).
[20] T.Pichler, M.Knupfer, M.S.Golden, J.Fink, A.Rinzler, and R.E.Smalley, Phys. Rev. Lett. **80**, 4729 (1998).
[21] A.G.Marinopoulos, L.Reining, A.Rubio, and N.Vast, Phys. Rev. Lett. **91**, 046402 (2003).
[22] I.V.Bondarev, L.M.Woods, and K.Tatur, Phys. Rev. B **80**, 085407 (2009).
[23] I.V.Bondarev, L.M.Woods, and A.Popescu, *Plasmons: Theory and Applications* (Nova Science, NY, 2011). Ch.16, p.381.
[24] I.V.Bondarev, Phys. Rev. B **85**, 035448 (2012).
[25] I.V.Bondarev and T.Antonijevic, Phys. Stat. Sol. C **9**, 1259 (2012).
[26] I.V.Bondarev and A.V.Meliksetyan, Phys. Rev. B **89**,

045414 (2014).
[27] A.Popescu, L.M.Woods, and I.V.Bondarev, Phys. Rev. B **83**, 081406(R) (2011).
[28] L.M.Woods, A.Popescu, D.Drosdoff, and I.V.Bondarev, Chem. Phys. **413**, 116 (2013).
[29] I.V.Bondarev and Ph.Lambin, Phys. Rev. B **72**, 035451 (2005); Solid State Commun. **132**, 203 (2004).
[30] I.V.Bondarev and Ph.Lambin, in *Trends in Nanotubes Research*, D.A.Martin, ed. (Nova Science, NY, 2006), Ch.6, p.139.
[31] I.V.Bondarev and Ph.Lambin, Phys. Rev. B **70**, 035407 (2004); Phys. Lett. A **328**, 235 (2004).
[32] I.V.Bondarev and B.Vlahovic, Phys. Rev. B **74**, 073401 (2006).
[33] I.V.Bondarev, Optics Express **23**, 3972 (2015).
[34] I.V.Bondarev and B.Vlahovic, Phys. Rev. B **75**, 033402 (2007).
[35] M.F.Gelin, I.V.Bondarev, and A.V.Meliksetyan, Chem. Phys. **413**, 123 (2013).
[36] M.F.Gelin, I.V.Bondarev, and A.V.Meliksetyan, J. Chem. Phys. **140**, 064301 (2014).
[37] I.V.Bondarev, J. Comp. Theor. Nanosci. **7**, 1673 (2010).
[38] I.V.Bondarev, J. Electron. Mater. **36**, 1579 (2007).
[39] I.V.Bondarev, M.F.Gelin, and A.V.Meliksetyan, in *Dekker Encyclopedia of Nanosci. and Nanotechn.*, S.E.Lyshevski, ed. (3rd ed., CRC, NY, 2014), p.4989.
[40] M.V.Kharlamova, Phys. Uspekhi **56**, 1047 (2013).
[41] N.Karousis, N.Tagmatarchis, and D.Tasis, Chem. Rev. **110**, 5366 (2010).
[42] S.Cambré, J.Campo, C.Beirnaert, C.Verlackt, P.Cool, and W.Wenseleers, Nature Nanotechn. **10**, 248 (2015).
[43] S.Cambré and W.Wenseleers, Angew. Chem. **123**, 2816 (2011).
[44] T.Takenobu, T.Takano, M.Shiraishi, Y.Murakami, M.Ata, H.Kataura, Y.Achiba, and Y.Iwasa, Nature Mater. **2**, 683 (2003).
[45] L.Duclaux, Carbon **40**, 1751 (2002).
[46] M.Olek, T.Busgen, M.Hilgendorff, M.Giersig, J. Phys. Chem. B **110**, 12901 (2006).
[47] J.M.Haremza, M.A.Hahn, T.D.Krauss, NanoLett. **2**, 1253 (2002).
[48] G.-H.Jeong, A.A.Farajian, R.Hatakeyama, T.Hirata, T.Yaguchi, K.Tohji, H.Mizuseki, and Y.Kawazoe, Phys. Rev. B **68**, 075410 (2003); Thin Solid Films **435**, 307 (2003).
[49] M.Khazaei, A.A.Farajian, G.-H.Jeong, H.Mizuseki, T.Hirata, R.Hatakeyama, and Y.Kawazoe, J. Phys. Chem. B **108**, 15529 (2004).
[50] Y.Zhao, J.Wei, R.Vajtai, P.M.Ajayan, and E.V.Barrera, Sci. Rep. **1**, 83 (2011).
[51] A.A.Eliseev, M.V.Kharlamova, M.V.Chernysheva, A.V. Lukashin, Yu.D.Tretyakov, A.S.Kumskov, and N.A.Kiselev, Russian Chem. Rev. **78**, 833 (2009).
[52] A.A.Eliseev, L.V.Yashina, N.I.Verbitskiy, M.M.Brzhezinskaya, M.V.Kharlamova, M.V.Chernysheva, A.V.Lukashin, N.A.Kiselev, A.S.Kumskov, B.Freitag, A.V.Generalov, A.S.Vinogradov, Y.V.Zubavichus, E.Kleimenov, and M.Nachtegaal, Carbon **50**, 4021 (2012).
[53] A.Ilie, J.S.Bendall, K.Nagaoka, S.Egger, T.Nakayama, and S.Crampin, ACS Nano **5**, 2559 (2011).
[54] R.Kitaura, R.Nakanishi, T.Saito, H.Yoshikawa, K.Awaga, and H.Shinohara, Angew. Chem. Int. Ed. **48**, 8298 (2009).
[55] C.Cuerret-Piécourt, Y.Le Bouar, A.Loiseau, and H.Pascard, Nature **372**, 761 (1994).
[56] N.Grobert, W.K.Hsu, Y.Q.Zhu, J.P.Hare, H.W.Kroto, D.R.M.Walton, M.Terrones, H.Terrones, Ph.Redlich, M.Rühle, R.Escudero, and F.Morales, Appl. Phys. Lett. **75**, 3363 (1999).
[57] A.Leonhardt, A.Ritschel, R.Kozhuharova, A.Graff, T.Mühl, R.Huhle, I.Mönch, D.Elefant, and C.M.Schneider, Diamond Relat. Mater. **12**, 790 (2003).
[58] N.Grobert, M.Terrones, A.J.Osborne, H.Terrones, W.K. Hsu, S.Trasobares, Y.Q.Zhu, J.P.Hare, H.W.Kroto, and D.R.M.Walton, Appl. Phys. A **67**, 595 (1998).
[59] A.A.Setlur, J.M.Lauerhaas, J.Y.Dai, and R.P.H.Chang, Appl. Phys. Lett. **69**, 345 (1996).
[60] A.Loiseau and H.Pascard, Chem. Phys. Lett. **256**, 246 (1996).
[61] L.H.Guan, K.Suenaga, Z.J.Shi, Z.N.Gu, and S.Iijima, NanoLett. **7**, 1532 (2007).
[62] L.Guan, K.Suenaga, S.Okubo, T.Okazaki, and S.Lijima, J. Am. Chem. Soc. **130**, 2162 (2008).
[63] R.Kitaura, N.Imazu, K.Kobayashi, and H.Shinohara, NanoLett. **8**, 693 (2008).
[64] V.Meunier, H.Muramatsu, T.Hayashi, Y.A.Kim, D.Shimamoto, H.Terrones, M.S.Dresselhaus, M.Terrones, M.Endo, and B.G.Sumpter, NanoLett. **9**, 1487 (2009).
[65] H.Muramatsu, T.Hayashi, Y.A.Kim, D.Shimamoto, M.Endo, M.Terrones, and M.S.Dresselhaus, NanoLett. **8**, 237 (2008).
[66] R.Nakanishi, R.Kitaura, P.Ayala, H.Shiozawa, K.de Blauwe, P.Hoffmann, D.Choi, Y.Miyata, T.Pichler, and H.Shinohara, Phys. Rev. B **86**, 115445 (2012).
[67] R.Hatakeyama and Y.F.Li, J. Appl. Phys. **102**, 034309 (2007).
[68] C.-K.Yang, J.Zhao, and J.P.Lu, Phys. Rev. Lett. **90**, 257203 (2003).
[69] V.V.Ivanovskaya, C.Köhler, and G.Seifert, Phys. Rev. B **75**, 075410 (2007).
[70] J.-H.Parq, J.Yu, and G.Kim, J. Chem. Phys. **132**, 054701 (2010).
[71] J.Kazerovskis, S.Piskunov, Y.F.Zhukovskii, P.N.D'yachkov, and S.Bellucci, Chem. Phys. Lett. **577**, 92 (2013).
[72] C.Jo and J.I.Lee, J. Magn. and Magn. Mater. **320**, 3256 (2008).
[73] C.Jo, J. Phys. D **42**, 105008 (2009).
[74] J.Zhou, X.Yan, G.Luo, R.Qin, H.Li, J.Lu, W.N.Mei, and Z.Gao, J. Phys. Chem. C **114**, 15347 (2010).
[75] A.Garcia-Fuente, V.M.Garcia-Suarez, J.Ferrer, and A.Vega, J. Phys.: Condens. Matter **23**, 265302 (2011).
[76] Y.Min, K.L.Yao, Z.L.Liu, G.Y.Gao, H.G.Cheng, and S.C.Zhu, Nanotechn. **20**, 095201 (2009).
[77] Y.Toyozawa, *Optical Processes in Solids* (Cambridge University Press, 2003).
[78] S.Tasaki, K.Maekawa, and T.Yamabe, Phys. Rev. B **57**, 9301 (1998).
[79] Z.M.Li, Z.K.Tang, H.J.Liu, N.Wang, C.T.Chan, R.Saito, S.Okada, G.D.Li, J.S.Chen, N.Nagasawa, and S.Tsuda, Phys. Rev. Lett. **87**, 127401 (2001).
[80] I.V.Bondarev, G.Ya.Slepyan, and S.A.Maksimenko, Phys. Rev. Lett. **89**, 115504 (2002).
[81] A.S.Davydov, *Quantum Mechanics* (NEO, Ann Arbor, MI, 1967).
[82] L.C.Andreani, G.Panzarini, and J.-M.Gérard, Phys. Rev. B **60**, 13276 (1999).
[83] A.Sharma, V.Singh, T.L.Bougher, and B.A.Cola, Nature Nanotechn., DOI:10.1038/nnano.2015.220
[84] M.Barkelid and V.Zwiller, Nature Photon. **8**, 47 (2014).

[85] S.Nanot, A.W.Cummings, C.L.Pint, A.Ikeuchi, T.Akiho, K.Sueoka, R.H.Hauge, F.Leonard, and J.Kono, Sci. Rep. **3**, 1335 (2013).

[86] S.Frank, P.Poncharal, Z.L.Wang, and W.A.de Heer, Science **280**, 1744 (1998).

[87] V.Mujica, M.Kemp, M.A.Ratner, J. Chem. Phys. **101**, 6849 (1994).

[88] V.Mujica, M.Kemp, M.A.Ratner, J. Chem. Phys. **101**, 6856 (1994).

[89] M.F.Gelin, Z.Li, and D.S.Kosov, J. Chem. Phys. **124**, 104703 (2006).

[90] G.Mahan, *Many-Particle Physics* (Plenum, NY, 2000).

[91] A.E.Miroshnichenko, S.Flach, and Y.S.Kivshar, Rev. Mod. Phys. **82**, 2257 (2010).

[92] E.G.Petrov and P.Hänggi, Phys. Rev. Lett. **86**, 2862 (2001).

[93] F.Leonard and J.Tersoff, Phys. Rev. Lett. **84**, 4693 (2000).

[94] Y.Xue and M.A.Ratner, Phys. Rev. B **69**, 161402(R) (2004).

[95] V.Perebeinos and J.Tersoff, Nano Lett. **14**, 4376 (2014).

[96] Y.-Z.Ma, C.D.Spataru, L.Valkunas, S.G.Louie, and G.R.Fleming, Phys. Rev. B **74**, 085402 (2006).

[97] R.B.Capaz, C.D.Spataru, S.Ismail-Beigi, and S.G.Louie, Phys. Rev. B **74**, 121401R (2006).

[98] L.A.Girifalco, *Statistical Mechanics of Solids* (Oxford University Press, NY, 2000).

[99] C.Kittel, *Introduction to Solid State Physics* (J.Wiley & Sons, NY, 2005).

[100] E.G.Emberly and G.Kirczenow, Phys. Rev. B **61**, 5740 (2000).

[101] S.Piscanec, M.Lazzeri, J.Robertson, A.C.Ferrari, and F.Mauri, Phys. Rev. B **75**, 035427 (2007).

[102] V.Perebeinos and Ph.Avouris, NanoLett. **7**, 609 (2007).

[103] S.Datta, T.Saha-Dasgupta, and A.Mookerjee, Eur. Phys. J. B **66**, 57 (2008).

[104] Y.Xu, X.Shi, Z.Zeng, Z.Y.Zeng, and B.Li, J. Phys.: Condens. Matter **19**, 056010 (2007).

[105] P.A.Khomyakov and G.Brocks, Phys. Rev. B **70**, 195402 (2004).

[106] R.H.M.Smit, C.Untiedt, G.Rubio-Bollinger, R.C.Segers, and J.M.van Ruitenbeek, Phys. Rev. Lett. **91**, 076805 (2003).

[107] N.D.Lang and Ph.Avouris, Phys. Rev. Lett. **81**, 3515 (1998).

[108] D.A.Ryndyk and G.Cuniberti, Phys. Rev. B **76** 155430 (2007).

[109] D.Nozaki, H.M.Postawski, and G.Cuniberti, New J. Phys. **12**, 063004 (2010).

[110] G.Cuniberti, F.Grossmann, and R.Gutiérrez, Adv. Solid State Phys. **42**, 133 (2002).

[111] D.Nozaki, Y.Girard, and K.Yoshizawa, J. Phys. Chem. C **112**, 17408 (2008).

[112] *CRC Handbook of Chemistry and Physics*, W.M.Haynes, D.R.Lide, and T.J.Bruno, eds. (Taylor & Francis, NY, 2015).

[113] J.M.Ziman, *Principles of the Theory of Solids*, 2nd edn. (Cambridge University Press, NY, 1972).

[114] V.Mujica, A.Nitzan, S.Datta, M.A.Ratner, C.P.Kubiak, J. Phys. Chem. B **107**, 91 (2003).

[115] A.W.Ghosh, T.Rakshit, and S.Datta, NanoLett. **4**, 565 (2004).

[116] C.D.Spataru and F.Leonard, Phys. Rev. Lett. **104**, 177402 (2010).

[117] G.Doetsch, *Guide to the Applications of the Laplace and Z-Transforms*, Van Nostrand Reinhold Co., London, 1971. [See also http://eqworld.ipmnet.ru/index.htm]